



Contents lists available at ScienceDirect

European Journal of Medicinal Chemistry

journal homepage: <http://www.elsevier.com/locate/ejmech>

Original article

Development of selective DprE1 inhibitors: Design, synthesis, crystal structure and antitubercular activity of benzothiazolylpyrimidine-5-carboxamides



Rupesh Chikhale^{a,*}, Sunil Menghani^a, Ramavath Babu^b, Ratnadeep Bansode^c,
G. Bhargavi^b, Nazira Karodia^c, M.V. Rajasekharan^b, Anant Paradkar^c,
Pramod Khedekar^{a,c,**}

^a Computer Aided Drug Design Laboratory, Department of Pharmaceutical Sciences, Rashtrasant Tukadoji Maharaj Nagpur University, Mahatma Jyotiba Fuley Shaikshaniik Parisar, Amravati Road, Nagpur 440 033, MS, India

^b School of Chemistry, University of Hyderabad, C. R. Rao Road, Hyderabad 500 046, AP, India

^c Centre for Pharmaceutical Engineering Science, Faculty of Life Sciences, University of Bradford, Richmond Road, Bradford BD7 1DP, West Yorkshire, United Kingdom

ARTICLE INFO

Article history:

Received 11 January 2015

Received in revised form

2 April 2015

Accepted 4 April 2015

Available online 7 April 2015

Keywords:

Benzothiazole

DprE1 inhibitors

Crystal structure

Molecular docking

3D-QSAR

Pharmacophore modelling

ABSTRACT

Decaprenylphosphoryl-b-d-ribose 20-epimerase (DprE1) is a potential drug target for development of antitubercular agents. Structure based drug discovery approach yielded twenty novel derivatives of benzothiazolylpyrimidine-5-carboxamides (**7a–t**) which were synthesised by three component one pot reaction involving benzothiazolyl oxobutanamide, thiourea and substituted aromatic benzaldehydes. These derivatives were evaluated for antitubercular activity to determine MIC and compound **7a**, **7e**, **7f** and **7o** were found to be potentially active against *Mycobacterium tuberculosis* (H₃₇Rv). Log P of these compounds was found to be between 2.0 and 3.0 making them suitable for oral dosing. DprE1 selectivity and pharmacokinetic studies were carried out for these compounds of which **7a** and **7o** were found to be highly selective and bioavailability was found to be above 52% by oral dose. Crystal structure of **7a** was studied and molecular packing was determined, it exhibited a triclinic crystal lattice arrangement having hydrogen bonded dimeric arrangement. Drug receptor interactions were studied which exhibited docking in the active site of receptor with hydrogen bonding, hydrophobic interactions, vdW interactions with amino acid residues such as Cys387, Asn385, Lys418, Tyr314, Gln334 and Lys367 respectively. 3D QSAR analysis was carried out by kNN-MFA method to determine and develop theoretical model, best suitable model was found to be based on Simulated Annealing k-Nearest Neighbour Molecular Field Analysis (SA kNN-MFA). The model provided with hydrophobic descriptors in positive side indicating the need of bulky groups, steric and electronegative descriptors in negative coordinates hints with contribution by the electronegative substitutions as favourable and desirable moieties for enhancing the activity. The q², q²_{se} and Pred_r²_{se} were found to be 0.5000, 0.6404 and 1.0094 respectively. A pharmacophore model was generated which suggested for necessity of aromatic, aliphatic carbon centre and hydrogen bond donor for development of newer DprE1 selective inhibitors.

© 2015 Elsevier Masson SAS. All rights reserved.

* Corresponding author.

** Corresponding author. Computer Aided Drug Design Laboratory, Department of Pharmaceutical Sciences, Rashtrasant Tukadoji Maharaj Nagpur University, Mahatma Jyotiba Fuley Shaikshaniik Parisar, Amravati Road, Nagpur 440 033, MS, India.

E-mail addresses: rupeshchikhale7@gmail.com (R. Chikhale), pbkhedekarudps@gmail.com (P. Khedekar).

1. Introduction

Tuberculosis (TB) is an infectious disease that spreads through air, mostly affecting young adults in their productive years. About 95% TB deaths are in the developing world of which 38% occurs in India and China. In 2010, about 650,000 cases were estimated for multidrug-resistant TB (MDR-TB) and an estimated 150,000 MDR-TB deaths were estimated annually in 2008 [1]. Prior to 1944 there was no medicine for TB and since last 50 years no new drug

Abbreviations

TB	tuberculosis
MDR-TB	multidrug-resistant TB
XDR-TB	extensively drug-resistant TB
DprE1	decaprenyl phosphoryl-b-D-ribose 20-epimerase
SBDD	structure based drug discovery
MIC	minimal inhibitory concentration
MBC	minimal bactericidal concentration
CFU	colony forming unit
DCPIP	2,6-dichlorophenolindophenol
k-NN SVS	k-nearest neighbour-stepwise variable selection
k-NN GA	k-nearest neighbour-genetic algorithm
k-NN SA	k-nearest neighbour-simulated annealing

entered market for treatment of TB except Bedaquiline [2]. There has been rise in drug-resistant TB due to inadequate treatment and non-compliance by patient. It has led to more dangerous form of condition as the TB bacilli becomes resistant to Isoniazid and Rifampicin, the two most powerful anti-TB drugs. Another threat from TB is the rise of extensively drug-resistant (XDR) TB, particularly in immune compromised patients such as in HIV making the scenario worse and calls for development of newer drugs to control this TB epidemic [3,4].

Cell wall is a functional and protective interface between external and internal environment for every living cell. Disruption or inhibition in its synthesis prevents the growth and multiplication of the organism. Targeting the cell wall synthesis has been a successful approach in drug development. The causative microorganism *Mycobacterium tuberculosis* (*M. tuberculosis*) has a special cell wall arrangement, with layers of outer lipids, mycolic acid, polysaccharides (arabinogalactan), peptidoglycan, plasma membrane, lipoarabinomannan (LAM), and phosphatidylinositol mannoside. The polysaccharides (arabinogalactans) are basic precursor for bacterial cell wall synthesis, Decaprenyl phosphoryl-b-D-ribose 20-epimerase (DprE1) is an oxidase involved in the biosynthesis of decaprenylphosphoryl-D-arabinose (DPA). It acts as donor of D-arabinofuranosyl residues for the synthesis of arabinogalactan. DprE1 is a flavoprotein that along with decaprenylphosphoryl-2-keto-ribose reductase (DprE2) catalyses epimerization of decaprenylphosphoryl-D-ribose (DPR) to decaprenylphosphoryl-D-arabinose (DPA) through an intermediate formation of decaprenylphosphoryl-2-Keto-ribose (DPX) (Fig. 1). This NADP dependent enzymatic reaction makes DprE1 an essential component for cell growth and survival, thus making it a potential drug target [5,6].

Several reports have shown that benzothiazin-4-ones (BTZs) is a promising class of DprE1 inhibitors against drug-susceptible and MDR/XDR strains of *M. tuberculosis*. However, poor pharmacokinetic and inferior physicochemical properties of these compounds directed us for development of newer compounds (Fig. 2) [7].

Benzothiazine derivative BTZ043 and its racemate BTZ038 has been reported as most active DprE1 inhibitor to date with minimum inhibitory concentration (MIC) of 1 ng/ml against the pathological strain. Further development of benzothiazine derivatives was reported for improved pharmacokinetic and physicochemical parameter based on structure activity relationship studies (SAR) [8]. Fig. 2 exhibits various compounds with DprE1 inhibiting action leading to antitubercular activity. Wang et al., reported a benzothiazolyl derivative (TCA1) as selective inhibitor of DprE1 leading to cell wall inhibition. This prompted us for the development of benzothiazole and pyrimidine derivatives as selective inhibitor of

the DprE1 inhibitor on basis of Structure Based Drug Discovery (SBDD) model [15]. The present article reports design of fused benzothiazolylpyrimidine derivatives based on the homology modelling, molecular docking and quantitative structure activity relationship (QSAR) studies with DprE1 as target protein.

The crystal structure of DprE1 for *M. tuberculosis* was described recently in bound form with BTZ043 and TCA1 by Batt et al. [16], and Wang et al. [15], respectively. The conversion of DPR to DPX is catalysed by enzyme DprE1 which is an example of FAD-dependent oxidation catalysis. This implies that flavin is reduced to FADH₂ and re-oxidised by either molecular oxygen or by organic mycobacterial membrane embedded electron acceptors like menaquinone. Earlier reports have disclosed that compounds with nitro group is converted to amino group by DprE1 which further covalently reacts with the Cys387 resulting into inactivation of the enzyme [8]. Wang et al., reported that TCA1 binds DprE1 noncovalently at the Cys387 and Tyr314 making hydrophobic and van der Waals contacts of shorter distances resulting in enzyme inhibition. Earlier we have reported the synthesis and pharmacological activities of pyrimidines and benzothiazoles along with mycobacterial restraining properties of benzothiazolyl derivatives on DprE1 and AcetoHydroxy Acid Synthase (AHAS) especially for control of *M. Tuberculosis* [17–20]. Herein, we report design, synthesis and antitubercular activity of benzothiazolyl pyrimidines based on noncovalent interactions with the target enzyme DprE1 along the active site, which is proved by enzyme specific assay and molecular docking study. We attempted to establish structure activity relationship (SAR) on the basis of 3D-QSAR studies and development of a pharmacophore model from the compounds of this series.

2. Chemistry

The lead molecule ethyl ({2-[(1, 3-benzothiazol-2-yl)carboxyl]amino} thiophen-3-yl)carbonyl carbamate (TCA1) have benzothiazolyl nucleus linked to thiophene moiety [15]. Benzothiazolyl nucleus conjugated with heterocyclic rings has shown potent activity as antibacterial compounds. To develop compounds with better antitubercular activity enhanced pharmacokinetic and physicochemical properties we designed benzothiazoles fused with pyrimidines. The classical Biginelli one pot three component reaction provides for interaction between an aldehyde, ester and binucleophile such as urea, thiourea or guanidine, this provides for variety of substitutions for designing of molecules based on molecular docking [17,21].

The designed synthesis involved acid catalysed one pot three component reaction of benzothiazolyl oxobutanamide, substituted aryl aldehydes and thiourea to yield benzothiazolyl tetrahydro-6-methyl-4-substituted phenyl-2-thioxopyrimidine-5-carboxamide derivatives (Scheme 1). Reactions were carried out in three steps; in first step 2-aminobenzothiazole was obtained from aniline **1** via formation of phenyl thiourea **2** in presence of HCl, it then undergoes cyclization in presence of bromine to yield 2-aminobenzothiazole **3**. 2-Aminobenzothiazole reacts with ethyl acetoacetate to yield benzothiazolyl oxobutanamide **4**, which further undergoes Biginelli one pot condensation reaction in presence of substituted benzaldehydes **5** and thiourea **6** to yield twenty derivatives **7a–t**.

3. Antitubercular studies

3.1. In vitro studies

3.1.1. Minimal inhibitory concentration (MIC), minimal bactericidal concentration (MBC) and DprE1 inhibitory studies

The newly synthesized compounds were evaluated for their

antitubercular activity by determining the MIC and MBC. Synthesized compounds **7a–t** was subjected to *in vitro* screening according to methods established by Jayaram *et al* [22] and Marry *et al.* [23]. The DprE1 inhibitory studies were carried out by the method reported by Neres *et al.* for the compounds **7a**, **7e**, **7f** and **7o** which were found to be most active on the basis of MIC.

3.2. *In vivo* studies

3.2.1. Physicochemical and pharmacokinetic studies

The physicochemical properties (Log *P*) of compounds **7a**, **7e**, **7f** and **7o** were determined following method described by Takics-Novfik and Avdeef (Shake Flask method) [24]. The pharmacokinetic properties were investigated following the procedure reported by Gao *et al.*, the Sprague Dawley rats were administered single oral dose (p.o.) and intra venous (i.v.) dose of compound for determination of plasma concentration of the test compound [24,25].

4. Experimental section

4.1. Chemistry

Chemicals were obtained from Sigma Aldrich, Germany and Alfa Aeser, United Kingdom. Melting points (m.p.) were detected with open capillaries using Thermo Precision Melting point cum Boiling point apparatus (C-PMB-2, Mumbai, India) and are uncorrected. IR spectra (KBr) were recorded on FTIR-8400s spectrophotometer (Shimadzu, Japan). ¹H and ¹³C NMR was obtained using a Bruker Advance-II 400 Spectrometer on 400 MHz using tetramethylsilane (TMS) as internal standard. All chemical shift values were recorded as δ (ppm), coupling constant value *J* is measured in hertz, the peaks are presented as s (singlet), d (doublet), t (triplet), brs (broad singlet), dd (double doublet), m (multiplet). The purity of compounds was controlled by thin layer chromatography (Merck, silica gel, HF254–361, type 60, 0.25 mm, Darmstadt, Germany). X-ray data was collected on a BRUKER-AXS SMART APEX CCD X-ray

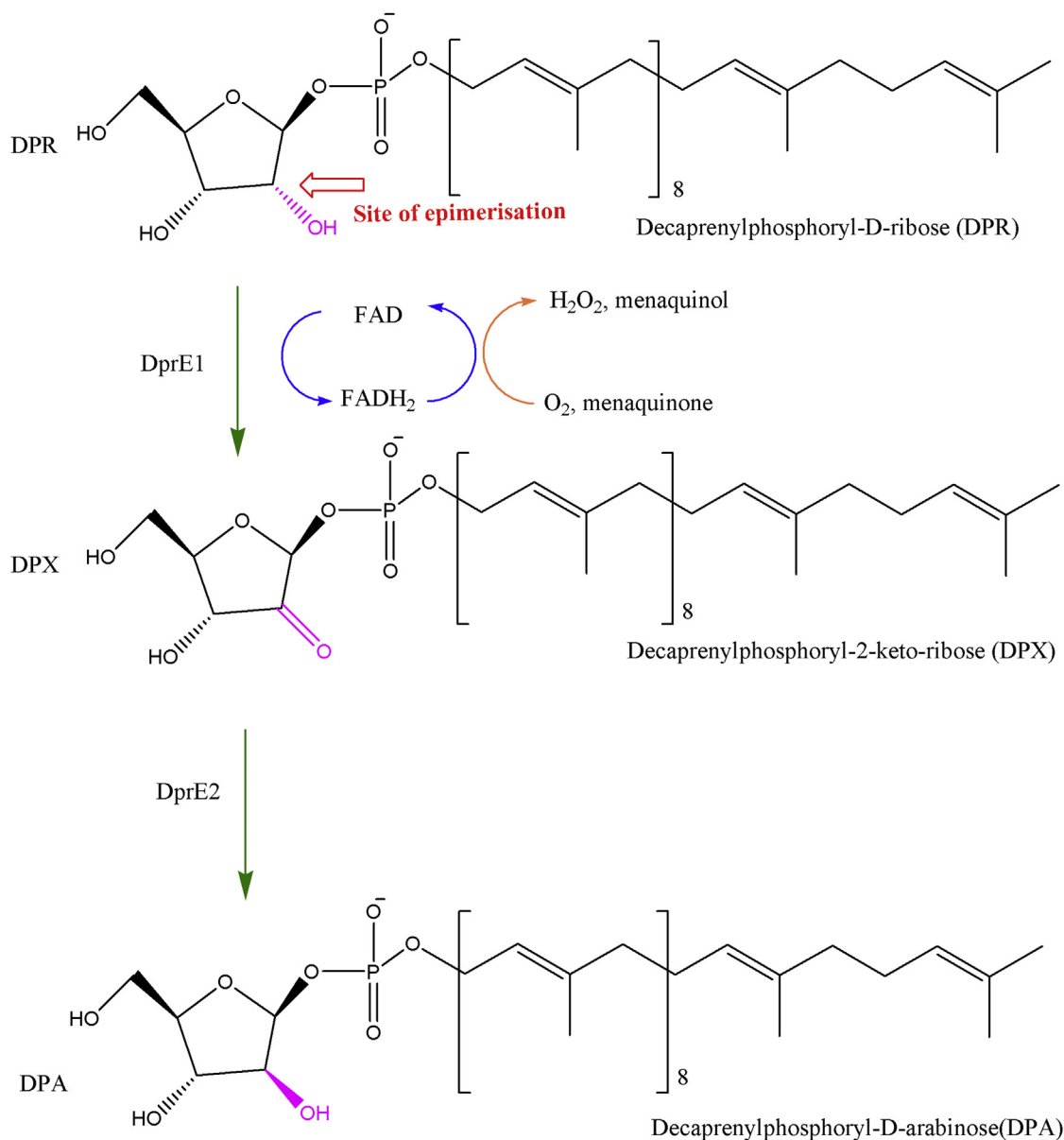


Fig. 1. The FAD dependent reaction catalysed by the DprE1 and DprE2 enzymes. The arrow indicates the position of 2'-OH, which is the site for epimerization leading to conversion of DPR to DPX to DPA. It is an oxidoreductase reaction having an interconversion of the FAD to FADH₂ re-oxidised by means of menaquinone or molecular oxygen.

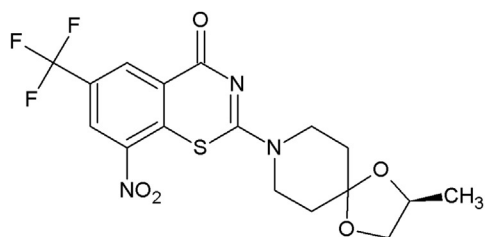
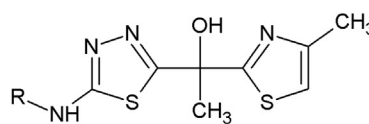
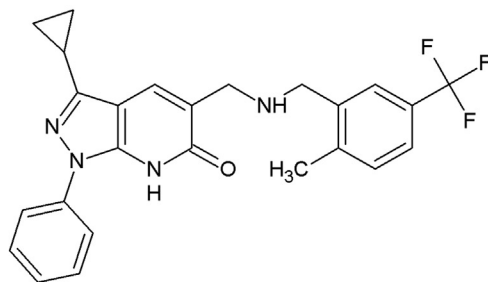
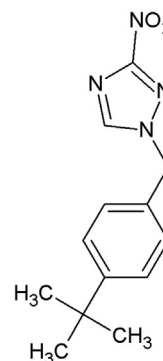
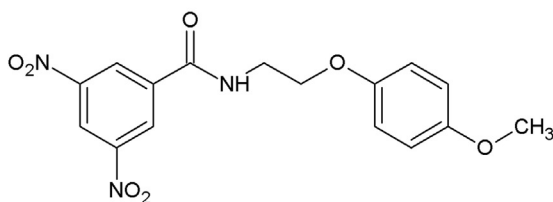
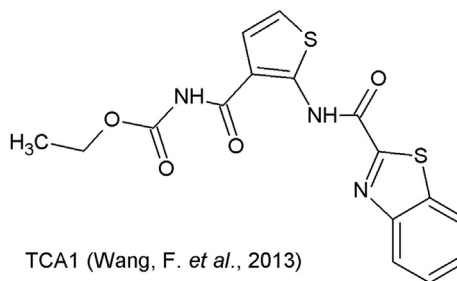
BTZ043 (Makarov, *et al.*, 2009)Methylthiazoles (Shirude, P. S., *et al.*, 2013)Pyrazolopyridones (Panda, M., *et al.*, 2014)377790 (Stanley *et al.*, 2012)DNB1 (Christophe *et al.*, 2009)TCA1 (Wang, F. *et al.*, 2013)

Fig. 2. Reported compounds targeting DprE1 exhibiting antitubercular activity [9–15].

diffractometer, using graphite-monochromatic Mo K α radiation ($= 0.71073 \text{ \AA}$). Mass spectra (ESI-MS) were recorded at Waters, Q-TOF LC-MS spectrometer (Waters, Micromass LC-MS, USA).

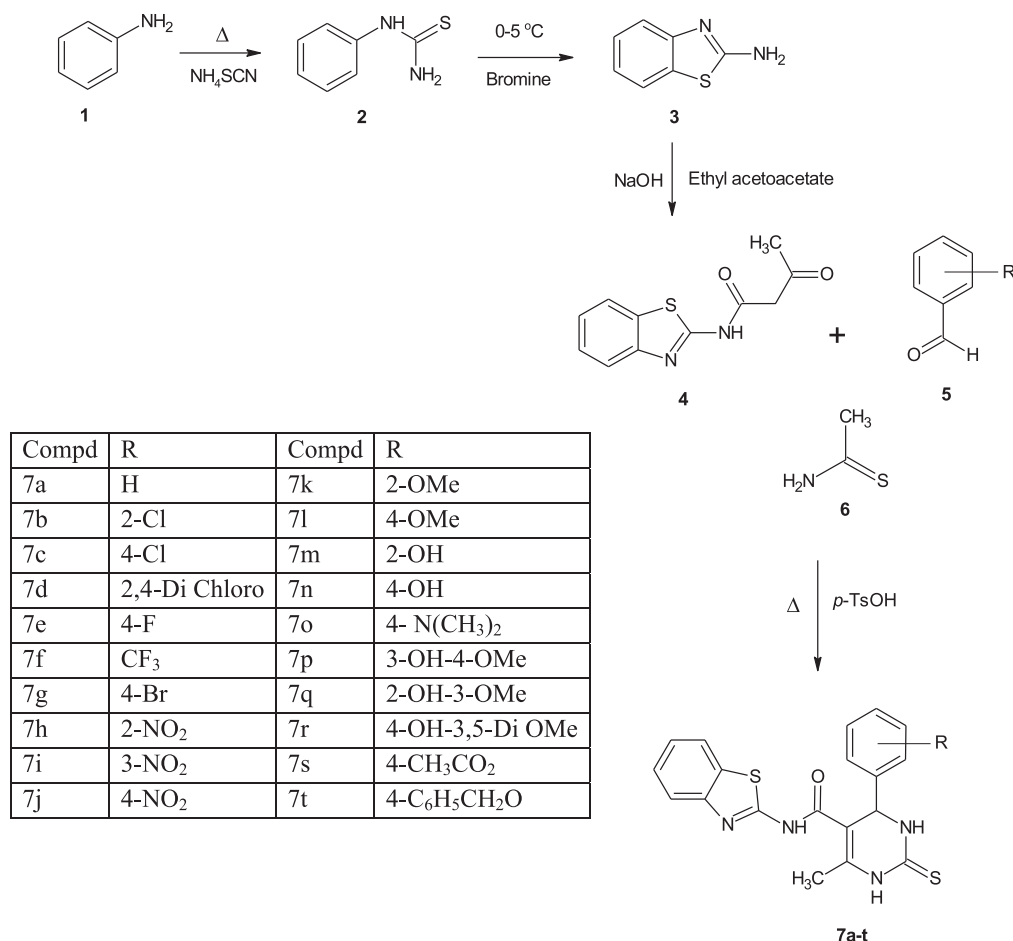
4.1.1. Procedure for synthesis of *N*-(benzo[d]thiazol-2-yl)-3-oxobutanamide (**4**)

A mixture of 2-aminobenzothiazole (10 mmol, 1.50 g) and ethyl acetoacetate (10 mmol, 1.31 ml) in 15 ml toluene was refluxed in the presence of catalytic amount of sodium hydroxide lye at 120 °C for 18 h, reaction was monitored on TLC. Toluene was distilled out and the resulting reaction mixture was washed with petroleum ether and diethyl ether thrice to obtain a free isolated yellow coloured compound **4**. The isolated product was recrystallized from methanol. Yield: 88%. m.p. 167–169 °C. IR (KBr) $\nu = 3343.58 \text{ cm}^{-1}$ (N–H), 1690.6 cm^{-1} (C=O), 1292.22 cm^{-1} (C–N). ^1H NMR (400 MHz, DMSO) δ 2.25 (s, 3H), 3.66 (s, 2H), 7.53 (t, $J = 6.98 \text{ Hz}$, 2H), 8.01 (d, $J = 8.4 \text{ Hz}$, 1H), 8.03 (d, $J = 8.1 \text{ Hz}$, 1H), 12.49 (s, 1H, N–H). ^{13}C NMR (100 MHz, DMSO) δ 29.9, 51.7, 118.3, 121.8, 124.5, 125.3, 130.8, 153.2, 164.0, 174.5, 202.8. ESI-MS m/z : calcd for $\text{C}_{11}\text{H}_{10}\text{N}_2\text{O}_2\text{S}$ found 234.27, $(\text{M}+\text{H})^+$: 235.04, $(\text{M}-\text{H})^-$: 232.02.

4.1.2. Typical procedure for synthesis of *N*-(benzo[d]thiazol-2-yl)-1,2,3,4-tetrahydro-6-methyl-4-substituted phenyl-2-thioxopyrimidine-5-carboxamide (**7a–t**)

To a mixture of **4** (10 mmol, 2.34 g), benzaldehyde (10 mmol, 1.06 g) and thiourea (10 mmol, 0.76 g) in methanol (20 ml) containing catalytic amount of *para*-toluene sulfonic acid (*p*-TsOH) was refluxed for about 12 h. After cooling to room temperature, the mixture was diluted with 150 ml of brine and extracted with ether ($2 \times 150 \text{ ml}$), dried over magnesium sulphate and excess of solvent was removed under reduced pressure. After complete drying the product was collected and recrystallized from DMF to obtain **7a–t**. The structure of compounds was confirmed by IR, ^1H and ^{13}C NMR and ESI-MS.

4.1.2.1. *N*-(benzo[d]thiazol-2-yl)-1,2,3,4-tetrahydro-6-methyl-4-phenyl-2-thioxopyrimidine-5-carboxamide (**7a**). This compound was obtained as yellow crystalline solid. Yield: 69%. m.p. 242–244 °C. IR (KBr) $\nu = 3112 \text{ cm}^{-1}$ (N–H str), 2926 cm^{-1} (methyl, C–H str-asy), 2853 cm^{-1} (C–H str-sym), 1671 cm^{-1} (amide C=O), 1505 cm^{-1} (C–N str), 1644, 1600, 1540, 1500 cm^{-1} (aromatic ring). ^1H NMR (400 MHz, DMSO) δ 2.48 (s, 3H, CH₃), 4.32 (s, 2H, N–H),



Scheme 1. Synthesis of N-(benzo[d]thiazol-2-yl)-1,2,3,4-tetrahydro-6-methyl-4-substituted phenyl-2-thioxopyrimidine-5-carboxamide derivatives.

5.29 (s, 1H, Pyrimidine), 7.14 (m, 2H), 7.23 (m, 2H), 7.30 (m, 2H), 7.37 (q, $J = 7.51$, 1H), 7.63 (m, 1H), 7.84 (m, 1H), 8.73 (s, 1H, N–H). ¹³C NMR (100 MHz, DMSO) δ 14.8, 55.7, 106.4, 121.9 (2), 124.5, 125.2, 125.9, 126.8, 127.0, 128.6 (2), 143.2, 149.0, 159.1 (2), 163.1, 174.5, 180.4. ESI-MS m/z : calcd for C₁₉H₁₆N₄OS₂ found 380.48 (M+H)⁺:381.11, (M–H)[–]: 378.95.

4.1.2.2. N-(benzo[d]thiazol-2-yl)-4-(2-chlorophenyl)-1,2,3,4-tetrahydro-6-methyl-2-thioxopyrimidine-5-carboxamide (**7b**). Yield: 72%. m.p. 236–238 °C. IR (KBr) $\nu = 3117$ cm^{–1} (N–H str), 2926 cm^{–1} (methyl, C–H str-asym), 2853 cm^{–1} (C–H str-sym), 1671 cm^{–1} (amide C=O), 1505 cm^{–1} (C–N str), 1330, 1325 cm^{–1} (C–Cl), 1644, 1600, 1540, 1500 cm^{–1} (aromatic ring). ¹H NMR (400 MHz, DMSO) δ 2.49 (s, 3H, CH₃), 4.3 (s, 2H, N–H), 5.38 (s, 1H, Pyrimidine), 7.24 (m, $J = 7.86$, 1H), 7.32 (m, $J = 8.26$, 2H), 7.35 (m, $J = 7.50$, 2H), 7.52 (t, $J = 8.9$, 1H), 7.68 (m, 2H), 8.2 (s, 1H, N–H). ¹³C NMR (100 MHz, DMSO) δ 15.2, 46.1, 106.4, 121.8, 121.9, 124.0, 125.2, 125.9, 126.7 (2), 128.2, 128.4, 128.7, 132.3, 142.8, 149.0, 163.1, 174.5(2). ESI-MS m/z : calcd for C₁₉H₁₅ClN₄O₂ found 414.93 (M+H)⁺: 416.03, (M–H)[–]: 412.9.

4.1.2.3. N-(benzo[d]thiazol-2-yl)-4-(4-chlorophenyl)-1,2,3,4-tetrahydro-6-methyl-2-thioxopyrimidine-5-carboxamide (**7c**). Yield: 68%. m.p. 243–245 °C. IR (KBr) $\nu = 3119$ cm^{–1} (N–H str), 2926 cm^{–1} (methyl, C–H str-asym), 2855 cm^{–1} (C–H str-sym), 1671 cm^{–1} (amide C=O), 1515 cm^{–1} (C–N str), 1335, 1325 cm^{–1} (C–Cl), 1644, 1600, 1540, 1500 cm^{–1} (aromatic ring). ¹H NMR

(400 MHz, DMSO) δ 2.49 (s, 3H, CH₃), 4.2 (s, 2H, N–H), 5.36 (s, 1H, Pyrimidine), 7.24 (t, $J = 7.56$, 1H), 7.37 (t, $J = 7.51$, 1H), 7.50 (t, $J = 8.29$, 2H), 7.52 (t, $J = 8.56$, 2H), 7.63 (t, $J = 8.26$, 1H), 7.8 (dd, $J = 3.63$, 1H) 8.4 (s, 1H, N–H). ¹³C NMR (100 MHz, DMSO) δ 15.8, 55.4, 106.4, 121.9 (2), 124.5, 125.4, 125.9, 128.4 (2), 128.7 (2), 132.3, 141.6, 149.0, 159.3, 163.1, 174.5 (2). ESI-MS m/z : calcd for C₁₉H₁₅ClN₄O₂ found 414.93 (M+H)⁺: 416.03; (M–1)[–]: 413.0.

4.1.2.4. N-(benzo[d]thiazol-2-yl)-4-(2,4-dichlorophenyl)-1,2,3,4-tetrahydro-6-methyl-2-thioxopyrimidine-5-carboxamide (**7d**). Yield: 71%. m.p. 231–233 °C. IR(KBr) $\nu = 3120$ cm^{–1} (N–H str), 2929 cm^{–1} (methyl, C–H str-asym), 2855 cm^{–1} (C–H str-sym), 1671 cm^{–1} (amide C=O), 1505 cm^{–1} (C–N str), 1332, 1328 cm^{–1} (C–Cl), 1644, 1600, 1540, 1500 cm^{–1} (aromatic ring). ¹H NMR (400 MHz, DMSO) δ 2.49 (s, 3H, CH₃), 4.1 (s, 2H, N–H), 5.47 (s, 1H, Pyrimidine), 7.17 (dd, $J = 7.51$, 1H), 7.24 (t, $J = 7.51$, 1H), 7.37 (m, 1H), 7.52 (m, 1H), 7.57 (t, $J = 7.51$, 1H), 7.63 (m, 1H), 7.8 (dd, $J = 7.51$, 1H), 8.4 (s, 1H, N–H). ¹³C NMR (100 MHz, DMSO) δ 15.5, 46.1, 106.4, 121.9 (2), 124.5, 125.2, 125.9, 126.8, 129.8, 130.2, 133.7 (2), 140.9, 149.0, 159.3, 163.4, 174.5 (2). ESI-MS m/z : calcd for C₁₉H₁₄Cl₂N₄O₂ found 449.37 (M+H)⁺: 450.50; (M–1)[–]: 446.89.

4.1.2.5. N-(benzo[d]thiazol-2-yl)-4-(4-fluorophenyl)-1,2,3,4-tetrahydro-6-methyl-2-thioxopyrimidine-5-carboxamide (**7e**). Yield: 63%. m.p. 247–249 °C. IR (KBr) $\nu = 3110$ cm^{–1} (N–H str), 2929 cm^{–1} (methyl, C–H str-asym), 2851 cm^{–1} (C–H str-sym), 1674 cm^{–1} (amide C=O), 1505 cm^{–1} (C–N str), 1150 cm^{–1} (C–F),

1645, 1600, 1540, 1500 cm^{-1} (aromatic ring). ^1H NMR (400 MHz, DMSO) δ 2.48 (s, 3H, CH_3), 4.32 (s, 2H, N–H), 5.36 (s, 1H, Pyrimidine), 7.07 (q, $J = 8.41$, 2H), 7.24 (t, $J = 7.21$, 1H), 7.33 (q, $J = 6.9$, 2H), 7.37 (m, 2H), 7.63 (m, 1H), 8.3 (s, 1H, N–H). ^{13}C NMR (100 MHz, DMSO) δ 15.2, 55.2, 106.4, 115.3 (2), 121.8, 121.9, 124.5, 125.2, 125.9, 128.6 (2), 138.8, 149.0, 159.1, 160.9, 163.1, 174.5 (2). ESI-MS m/z : calcd for $\text{C}_{19}\text{H}_{15}\text{FN}_4\text{O}_2\text{S}_2$ found 398.47 ($\text{M}+\text{H}$) $^+$: 400.06; ($\text{M}-1$) $^-$: 396.81.

4.1.2.6. *N*-(benzo[d]thiazol-2-yl)-4-(4-(trifluoromethyl)phenyl)-1,2,3,4-tetrahydro-6-methyl-2-thioxopyrimidine-5-carboxamide (**7f**). Yield: 68%. m.p. 239–241 °C. IR (KBr) $\nu = 3118$ cm^{-1} (N–H str), 2927 cm^{-1} (methyl, C–H str-*asym*), 2854 cm^{-1} (C–H str-*sym*), 1674 cm^{-1} (amide C=O), 1501 cm^{-1} (C–N str), 1155 cm^{-1} (C–F), 1645, 1600, 1540, 1501 cm^{-1} (aromatic ring). ^1H NMR (400 MHz, DMSO) δ 2.51 (s, 3H, CH_3), 4.1 (s, 2H, N–H), 5.31 (s, 1H, Pyrimidine), 7.24 (m, 2H), 7.37 (t, $J = 8.53$, 1H), 7.63 (m, 2H), 7.65 (s, 2H), 7.82 (dd, $J = 6.7$, 1H), 8.6 (s, 1H, N–H). ^{13}C NMR (100 MHz, DMSO) δ 15.4, 55.1, 106.4, 121.6, 121.9, 124.3, 124.5, 125.0 (2), 125.2, 125.9, 127.3 (2), 129.4, 146.5, 149.1, 159.2, 163.1, 174.5 (2). ESI-MS m/z : calcd for $\text{C}_{20}\text{H}_{15}\text{F}_3\text{N}_4\text{O}_2\text{S}_2$ found 448.48 ($\text{M}+\text{H}$) $^+$: 450.03; ($\text{M}-1$) $^-$: 446.94.

4.1.2.7. *N*-(benzo[d]thiazol-2-yl)-4-(4-bromophenyl)-1,2,3,4-tetrahydro-6-methyl-2-thioxopyrimidine-5-carboxamide (**7g**). Yield: 59%. m.p. 267–269 °C. IR (KBr) $\nu = 3118$ cm^{-1} (N–H str), 2923 cm^{-1} (methyl, C–H str-*asym*), 2855 cm^{-1} (C–H str-*sym*), 1675 cm^{-1} (amide C=O), 1505 cm^{-1} (C–N str), 450 cm^{-1} (C–Br) 1644, 1600, 1540, 1500 cm^{-1} (aromatic ring). ^1H NMR (400 MHz, DMSO) δ 2.50 (s, 3H, CH_3), 4.1 (s, 2H, N–H), 5.32 (s, 1H, Pyrimidine), 7.24 (m, 1H), 7.28 (m, 2H), 7.33 (m, 2H), 7.37 (m, 1H), 7.63 (q, $J = 7.01$, 1H), 7.8 (m, 1H), 8.6 (s, 1H, N–H). ^{13}C NMR (100 MHz, DMSO) δ 15.8, 55.3, 106.4, 121.8, 121.9, 124.4, 125.2, 125.9, 129.2 (2), 131.3, 131.5, 140.2, 149.0, 159.1, 163.1, 174.5 (2). ESI-MS m/z : calcd for $\text{C}_{19}\text{H}_{15}\text{BrN}_4\text{O}_2\text{S}_2$ found 459.38 ($\text{M}+\text{H}$) $^+$: 461.01; ($\text{M}-1$) $^-$: 457.98.

4.1.2.8. *N*-(benzo[d]thiazol-2-yl)-1,2,3,4-tetrahydro-6-methyl-4-(2-nitrophenyl)-2-thioxopyrimidine-5-carboxamide (**7h**). Yield: 66%. m.p. 231–233 °C. IR (KBr) $\nu = 3119$ cm^{-1} (N–H str), 2922 cm^{-1} (methyl, C–H str-*asym*), 2851 cm^{-1} (C–H str-*sym*), 1672 cm^{-1} (amide C=O), 1502 cm^{-1} (C–N str), 1375 cm^{-1} (C–NO₂), 1644, 1600, 1540, 1500 cm^{-1} (aromatic ring). ^1H NMR (400 MHz, DMSO) δ 2.52 (s, 3H, CH_3), 4.3 (s, 2H, N–H), 5.39 (s, 1H, Pyrimidine), 7.24 (t, $J = 8.53$, 1H), 7.37 (t, $J = 7.39$, 1H), 7.45 (m, 1H), 7.54 (t, $J = 7.9$, 1H), 7.63 (dd, $J = 7.5$, 1H), 7.71 (t, $J = 8.53$, 1H), 7.8 (d, $J = 8.1$, 1H), 8.07 (m, 1H), 8.9 (s, 1H, N–H). ^{13}C NMR (100 MHz, DMSO) δ 15.2, 55.2, 106.4, 121.8, 121.9, 124.4, 125.2, 125.9, 129.2 (2), 131.3, 131.5, 140.2, 149.0, 159.1, 163.1, 174.5 (2). ESI-MS m/z : calcd for $\text{C}_{19}\text{H}_{15}\text{N}_5\text{O}_3\text{S}_2$ found 425.48 ($\text{M}+\text{H}$) $^+$: 427.05; ($\text{M}-1$) $^-$: 423.52.

4.1.2.9. *N*-(benzo[d]thiazol-2-yl)-1,2,3,4-tetrahydro-6-methyl-4-(3-nitrophenyl)-2-thioxopyrimidine-5-carboxamide (**7i**). Yield: 84%. m.p. 244–246 °C. IR (KBr) $\nu = 3120$ cm^{-1} (N–H str), 2924 cm^{-1} (methyl, C–H str-*asym*), 2851 cm^{-1} (C–H str-*sym*), 1672 cm^{-1} (amide C=O), 1502 cm^{-1} (C–N str), 1375 cm^{-1} (C–NO₂), 1644, 1600, 1540, 1500 cm^{-1} (aromatic ring). ^1H NMR (400 MHz, DMSO) δ 2.49 (s, 3H, CH_3), 4.3 (s, 2H, N–H), 5.46 (s, 1H, Pyrimidine), 7.24 (t, $J = 8.5$, 1H), 7.37 (t, $J = 7.85$, 1H), 7.44 (t, $J = 8.7$, 1H), 7.63 (dd, $J = 8.2$, 1H), 7.8 (dd, $J = 8.4$, 1H), 7.87 (m, 1H), 8.03 (t, $J = 7.87$, 1H), 8.20 (m, 1H), 8.9 (s, 1H, N–H). ^{13}C NMR (100 MHz, DMSO) δ 15.2, 55.2, 106.4, 121.8, 121.9, 124.4, 125.2, 125.9, 129.2 (2), 131.3, 131.5, 140.2, 149.0, 159.1, 163.1, 174.5 (2). ESI-MS m/z : calcd for $\text{C}_{19}\text{H}_{15}\text{N}_5\text{O}_3\text{S}_2$ found 425.48 ($\text{M}+\text{H}$) $^+$: 427.05; ($\text{M}-1$) $^-$: 423.52.

4.1.2.10. *N*-(benzo[d]thiazol-2-yl)-1,2,3,4-tetrahydro-6-methyl-4-(4-nitrophenyl)-2-thioxopyrimidine-5-carboxamide (**7j**). Yield: 68%.

m.p. 230–232 °C. IR (KBr) $\nu = 3115$ cm^{-1} (N–H str), 2921 cm^{-1} (methyl, C–H str-*asym*), 2856 cm^{-1} (C–H str-*sym*), 1672 cm^{-1} (amide C=O), 1502 cm^{-1} (C–N str), 1378 cm^{-1} (C–NO₂), 1644, 1600, 1540, 1500 cm^{-1} (aromatic ring). ^1H NMR (400 MHz, DMSO) δ 2.48 (s, 3H, CH_3), 4.3 (s, 2H, N–H), 5.39 (s, 1H, Pyrimidine), 7.24 (m, 1H), 7.33 (dd, $J = 7.87$, 2H), 7.37 (dd, $J = 8.3$, 1H), 7.63 (m, 1H), 7.80 (m, 1H), 8.06 (dd, $J = 6.7$, 2H), 8.9 (s, 1H, N–H). ^{13}C NMR (100 MHz, DMSO) δ 15.2, 57.2, 106.4, 121.8, 122.9, 124.4, 125.2, 125.9, 129.2 (2), 131.3, 131.5, 140.2, 149.0, 159.1, 163.1, 174.5 (2). ESI-MS m/z : calcd for $\text{C}_{19}\text{H}_{15}\text{N}_5\text{O}_3\text{S}_2$ found 425.48 ($\text{M}+\text{H}$) $^+$: 427.05; ($\text{M}-1$) $^-$: 423.52.

4.1.2.11. *N*-(benzo[d]thiazol-2-yl)-1,2,3,4-tetrahydro-4-(2-methoxyphenyl)-6-methyl-2-thioxopyrimidine-5-carboxamide (**7k**). Yield: 67%. m.p. 256–258 °C. IR (KBr) $\nu = 3123$ cm^{-1} (N–H str), 2926 cm^{-1} (methyl, C–H str-*asym*), 2853 cm^{-1} (C–H str-*sym*), 1671 cm^{-1} (amide C=O), 1505 cm^{-1} (C–N str), 1402 cm^{-1} ($\text{CH}_3\text{--O--C}$), 1644, 1600, 1540, 1500 cm^{-1} (aromatic ring). ^1H NMR (400 MHz, DMSO) δ 2.1 (s, 3H, CH_3), 3.81 (s, 3H, OCH_3), 4.2 (s, 2H, N–H), 5.37 (s, 1H, Pyrimidine), 6.94 (t, $J = 7.46$, 1H), 7.04 (m, 1H), 7.23 (m, 2H), 7.37 (m, 1H), 7.63 (m, 1H), 7.8 (m, 2H), 8.7 (s, 1H, N–H). ^{13}C NMR (100 MHz, DMSO) δ 15.8, 45.3, 56.2, 106.4, 114.1, 120.9, 121.4, 121.8, 121.9, 124.5, 125.9, 127.8, 128.1, 149.0, 156.6, 159.1, 163.1, 174.5 (2). ESI-MS m/z : calcd for $\text{C}_{20}\text{H}_{18}\text{N}_4\text{O}_4\text{S}_2$ found 410.51 ($\text{M}+\text{H}$) $^+$: 412.02; ($\text{M}-1$) $^-$: 409.01.

4.1.2.12. *N*-(benzo[d]thiazol-2-yl)-1,2,3,4-tetrahydro-4-(4-methoxyphenyl)-6-methyl-2-thioxopyrimidine-5-carboxamide (**7l**). Yield: 77%. m.p. 226–228 °C. IR (KBr) $\nu = 3116$ cm^{-1} (N–H str), 2926 cm^{-1} (methyl, C–H str-*asym*), 2853 cm^{-1} (C–H str-*sym*), 1671 cm^{-1} (amide C=O), 1505 cm^{-1} (C–N str), 1402 cm^{-1} ($\text{CH}_3\text{--O--C}$), 1644, 1600, 1540, 1500 cm^{-1} (aromatic ring). ^1H NMR (400 MHz, DMSO) δ 1.26 (s, 3H, CH_3), 2.37 (s, 3H, OCH_3), 4.09 (s, 2H, N–H), 6.65 (s, 1H, Pyrimidine), 7.18 (q, $J = 8.44$, 2H), 7.24 (m, 1H), 7.28 (t, $J = 7.1$, 1H), 8.02 (t, $J = 7.1$, 1H), 8.17 (q, $J = 8.37$, 2H), 8.33 (m, 1H), 8.34 (m, 1H). ^{13}C NMR (100 MHz, DMSO) δ 15.8, 45.3, 56.2, 106.4, 114.1, 120.9, 121.3, 121.8, 121.9, 124.5, 125.0, 125.3, 127.8, 128.0, 149.1, 156.8, 159.1, 163.5, 174.5 (2). ESI-MS m/z : calcd for $\text{C}_{20}\text{H}_{18}\text{N}_4\text{O}_4\text{S}_2$ found 410.01 ($\text{M}+\text{H}$) $^+$: 412.12; ($\text{M}-1$) $^-$: 410.01.

4.1.2.13. *N*-(benzo[d]thiazol-2-yl)-1,2,3,4-tetrahydro-4-(2-hydroxyphenyl)-6-methyl-2-thioxopyrimidine-5-carboxamide (**7m**). Yield: 68%. m.p. 234–236 °C. IR (KBr) $\nu = 3132$ cm^{-1} (N–H str), 2922 cm^{-1} (methyl, C–H str-*asym*), 2916.12 cm^{-1} (O–H), 2855 cm^{-1} (C–H str-*sym*), 1669 cm^{-1} (amide C=O), 1501 cm^{-1} (C–N str), 1644, 1600, 1540, 1500 cm^{-1} (aromatic ring). ^1H NMR (400 MHz, DMSO) δ 1.26 (s, 3H, CH_3), 4.3 (s, 2H, N–H), 5.33 (s, 1H, Pyrimidine), 6.67 (m, 1H), 6.94 (t, $J = 8.29$, 1H), 7.24 (m, 1H), 7.37 (m, 2H), 7.38 (m, 1H), 7.63 (dd, $J = 7.3$, 1H), 7.8 (m, 1H), 8.5 (s, 1H, N–H), 10.1 (s, 1H, O–H). ^{13}C NMR (100 MHz, DMSO) δ 15.2, 45.0, 106.4, 115.7, 121.2, 121.8, 121.9, 122.9, 124.5, 125.2, 125.9, 128.2, 128.4, 149.0, 154.1, 159.1, 163.1, 175.5 (2). ESI-MS m/z : calcd for $\text{C}_{19}\text{H}_{16}\text{N}_4\text{O}_4\text{S}_2$ found 396.48 ($\text{M}+\text{H}$) $^+$: 397.07; ($\text{M}-1$) $^-$: 396.40.

4.1.2.14. *N*-(benzo[d]thiazol-2-yl)-1,2,3,4-tetrahydro-4-(4-hydroxyphenyl)-6-methyl-2-thioxopyrimidine-5-carboxamide (**7n**). Yield: 70%. m.p. 221–224 °C. IR (KBr) $\nu = 3129$ cm^{-1} (N–H str), 2922 cm^{-1} (methyl, C–H str-*asym*), 2916.12 cm^{-1} (O–H), 2855 cm^{-1} (C–H str-*sym*), 1669 cm^{-1} (amide C=O), 1501 cm^{-1} (C–N str), 1644, 1600, 1540, 1500 cm^{-1} (aromatic ring). ^1H NMR (400 MHz, DMSO) δ 2.14 (s, 3H, CH_3), 4.30 (s, 2H, N–H), 5.33 (s, 1H, Pyrimidine), 6.67 (m, 1H), 6.94 (t, $J = 8.29$, 1H), 7.24 (m, 1H), 7.37 (m, 2H), 7.38 (m, 1H), 7.63 (dd, $J = 7.3$, 1H), 7.8 (m, 1H), 8.5 (s, 1H, N–H), 10.1 (s, 1H, O–H). ^{13}C NMR (100 MHz, DMSO) δ 15.7, 45.2, 106.4, 115.8, 121.2, 121.8, 121.9, 122.9, 124.5, 125.2, 125.9, 128.2 (2), 149.0,

154.1, 159.1, 163.1, 175.5 (2). ESI-MS m/z : calcd for $C_{19}H_{16}N_4O_2S_2$ found 396.48 (M+H)⁺: 397.06; (M-1)⁻: 395.39.

4.1.2.15. *N*-(benzo[d]thiazol-2-yl)-4-(4-(dimethylamino)phenyl)-1,2,3,4-tetrahydro-6-methyl-2-thioxopyrimidine-5-carboxamide (**7o**). Yield: 76%. m.p. 230–232 °C. IR (KBr) ν = 3116 cm^{-1} (N–H str), 2926 cm^{-1} (methyl, C–H str-asym), 2853 cm^{-1} (C–H str-sym), 1671 cm^{-1} (amide C=O), 1505 cm^{-1} (C–N str), 1644, 1600, 1540, 1500 cm^{-1} (aromatic ring). ¹H NMR (400 MHz, DMSO) δ 2.32 (s, 3H, CH₃), 2.74 (s, 6H, N (CH₃)₂), 4.2 (s, 2H, N–H), 5.34 (s, 1H, Pyrimidine), 6.65 (q, J = 8.24, 2H), 7.09 (q, J = 7.89, 2H), 7.24 (t, J = 8.10, 1H), 7.37 (t, J = 8.4, 1H), 7.63 (m, 1H), 7.8 (m, 1H), 8.9 (s, 1H, N–H). ¹³C NMR (100 MHz, DMSO) δ 13.2, 40.3 (2), 55.2, 106.4, 114.1 (2), 121.8, 121.9, 124.5, 125.2, 125.9, 127.9 (2), 132.7, 147.6, 149.0, 159.1, 163.1, 174.5 (2). ESI-MS m/z : calcd for $C_{21}H_{21}N_5O_2S_2$ found 423.55 (M+H)⁺: 424.12; (M-1)⁻: 422.80.

4.1.2.16. *N*-(benzo[d]thiazol-2-yl)-1,2,3,4-tetrahydro-4-(3-hydroxy-4-methoxyphenyl)-6-methyl-2-thioxopyrimidine-5-carboxamide (**7p**). Yield: 77%. m.p. 251–253 °C. IR (KBr) ν = 3119 cm^{-1} (N–H str), 2920 cm^{-1} (methyl, C–H str-asym), 2852 cm^{-1} (C–H str-sym), 1675 cm^{-1} (amide C=O), 1506 cm^{-1} (C–N str), 1644, 1605, 1540, 1503 cm^{-1} (aromatic ring). ¹H NMR (400 MHz, DMSO) δ 2.49 (s, 3H, CH₃), 3.73 (s, 3H, OCH₃), 4.3 (s, 2H, N–H), 5.38 (s, 1H, Pyrimidine), 6.68 (d, J = 8.50, 1H), 6.72 (d, J = 2.49, 1H), 6.96 (q, J = 2.49, 1H), 7.42 (m, 1H), 7.37 (t, J = 7.51, 1H), 7.63 (m, 2H), 7.8 (m, 1H), 8.7 (s, 1H, N–H). ¹³C NMR (100 MHz, DMSO) δ 14.4, 55.5, 56.2, 106.4, 113.6, 115.5, 120.6, 121.8, 121.9, 124.5, 125.2, 125.9, 136.9, 145.5, 149.0, 149.4, 159.1, 163.1, 174.5 (2). ESI-MS m/z : calcd for $C_{20}H_{18}N_4O_3S_2$ found 426.51 (M+H)⁺: 427.08; (M-1)⁻: 425.98.

4.1.2.17. *N*-(benzo[d]thiazol-2-yl)-1,2,3,4-tetrahydro-4-(2-hydroxy-3-methoxyphenyl)-6-methyl-2-thioxopyrimidine-5-carboxamide (**7q**). Yield: 73%. m.p. 248–250 °C. IR (KBr) ν = 3119 cm^{-1} (N–H str), 2920 cm^{-1} (methyl, C–H str-asym), 2852 cm^{-1} (C–H str-sym), 1675 cm^{-1} (amide C=O), 1506 cm^{-1} (C–N str), 1644, 1605, 1540, 1503 cm^{-1} (aromatic ring). ¹H NMR (400 MHz, DMSO) δ 2.49 (s, 3H, CH₃), 3.79 (s, 3H, OCH₃), 4.3 (s, 2H, N–H), 5.32 (s, 1H, Pyrimidine), 6.65 (q, J = 8.6, 1H), 6.97 (q, J = 7.53, 1H), 7.09 (q, J = 7.53, 1H), 7.24 (t, J = 6.91, 1H), 7.37 (t, J = 7.51, 1H), 7.63 (m, 2H), 7.9 (m, 1H), 8.7 (s, 1H, N–H). ¹³C NMR (100 MHz, DMSO) δ 15.8, 55.5, 56.2, 106.4, 113.6, 115.5, 120.6, 121.8, 121.9, 124.5, 125.2, 125.9, 136.9, 145.5, 149.0, 149.4, 159.1, 163.1, 174.5 (2). ESI-MS m/z : calcd for $C_{20}H_{18}N_4O_3S_2$ found 426.51 (M+H)⁺: 427.07; (M-1)⁻: 425.96.

4.1.2.18. *N*-(benzo[d]thiazol-2-yl)-1,2,3,4-tetrahydro-4-(4-hydroxy-3,5-dimethoxyphenyl)-6-methyl-2-thioxopyrimidine-5-carboxamide (**7r**). Yield: 56%. m.p. 198–200 °C. IR (KBr) ν = 3121 cm^{-1} (N–H str), 2922 cm^{-1} (methyl, C–H str-asym), 2853 cm^{-1} (C–H str-sym), 1671 cm^{-1} (amide C=O), 1505 cm^{-1} (C–N str), 1402 cm^{-1} (CH₃–O–C) 1644, 1600, 1540, 1500 cm^{-1} (aromatic ring). ¹H NMR (400 MHz, DMSO) δ 2.49 (s, 3H, CH₃), 3.80 (s, 6H, OCH₃), 4.30 (s, 2H, N–H), 5.31 (s, 1H, Pyrimidine), 6.69 (s, 2H), 7.24 (t, J = 6.91, 1H), 7.37 (t, J = 7.51, 1H), 7.63 (m, 2H), 7.8 (m, 1H), 8.4 (s, 1H, N–H). ¹³C NMR (100 MHz, DMSO) δ 15.2, 55.8, 56.2 (2), 104.7 (2), 106.4, 121.8, 121.9, 124.5, 125.2, 125.9, 130.8, 137.8, 149.0, 152.2 (2), 159.1, 163.1, 174.5 (2). ESI-MS m/z : calcd for $C_{21}H_{20}N_4O_4S_2$ found 456.53 (M+H)⁺: 457.09; (M-1)⁻: 456.01.

4.1.2.19. Methyl-4-(5-(benzo[d]thiazol-2-yl)carbamoyl)-1,2,3,4-tetrahydro-6-methyl-2-thioxopyrimidin-4-ylbenzoate (**7s**). Yield: 59%. m.p. 220–222 °C. IR (KBr) ν = 3121 cm^{-1} (N–H str), 2918 cm^{-1} (methyl, C–H str-asym), 2854 cm^{-1} (C–H str-sym), 1674 cm^{-1} (amide C=O), 1505 cm^{-1} (C–N str), 1645, 1601, 1540, 1505 cm^{-1} (aromatic ring). ¹H NMR (400 MHz, DMSO) δ 2.09 (s, 3H,

acetyl), 2.49 (s, 3H, CH₃), 3.9 (s, 2H, N–H), 5.33 (s, 1H, Pyrimidine), 7.09 (m, 2H), 7.16 (m, 2H), 7.24 (t, J = 6.91, 1H), 7.37 (t, J = 5.49, 1H), 7.63 (m, 1H), 7.8 (m, 1H), 8.7 (s, 1H, N–H). ¹³C NMR (100 MHz, DMSO) δ 15.2, 20.3, 55.2, 106.4, 121.4, 121.8, 121.9, 125.2, 125.9, 127.4 (2), 140.0, 149.0, 159.1, 163.1, 169.0, 174.5(2). ESI-MS m/z : calcd for $C_{21}H_{18}N_4O_3S_2$ found 438.53 (M+H)⁺: 439.08; (M-1)⁻: 436.99.

4.1.2.20. *N*-(benzo[d]thiazol-2-yl)-4-(4-(benzyloxy)phenyl)-1,2-dihydro-6-methyl-2-thioxopyrimidine-5-carboxamide (**7t**). Yield: 72%. m.p. 256–258 °C. IR (KBr) ν = 3120 cm^{-1} (N–H str), 2920 cm^{-1} (methyl, C–H str-asym), 2850 cm^{-1} (C–H str-sym), 1677 cm^{-1} (amide C=O), 1510 cm^{-1} (C–N str), 1644, 1600, 1530, 1510 cm^{-1} (aromatic ring). ¹H NMR (400 MHz, DMSO) δ 2.49 (s, 3H, CH₃), 5.11 (s, 2H, CH₂), 4.3 (s, 2H, N–H), 5.34 (s, 1H, Pyrimidine), 7.14 (m, 1H), 7.17 (m, 2H), 7.24 (t, J = 8.42, 1H), 7.34 (m, 1H), 7.40 (m, 2H), 7.46 (m, 2H), 7.63 (m, 1H), 7.82 (m, 1H), 8.72 (s, 1H, N–H). ¹³C NMR (100 MHz, DMSO) δ 15.4, 55.2, 70.9, 106.4, 114.1 (2), 121.8, 121.9, 124.0, 125.2, 125.9, 127.2 (2), 128.0 (2), 129.0, 135.5, 141.2, 149.0, 158.7, 159.1, 163.1, 174.5 (2). ESI-MS m/z : calcd for $C_{26}H_{20}N_4O_2S_2$ found 484.57 (M+H)⁺: 4. 486.12; (M-1)⁻: 483.13.

4.2. Biological evaluation

All synthesised compounds were subjected to anti-tubercular activity against the pathogenic strain for *Mycobacterium tuberculosis* (H₃₇Rv) ATCC 27294.

4.2.1. In vitro anti-tubercular studies for determination of minimum inhibitory concentration (MIC) and minimal bactericidal concentration (MBC)

M. tuberculosis (Mtb) H₃₇Rv ATCC 27294 used for determination of MIC was cultured according to method reported previously by Jayaram et al. A single seed lot maintained at –70 °C was used for obtaining the inoculums for all the experiments. The bacteria was grown in roller bottles containing Middlebrook 7H9 broth supplemented with 0.2% glycerol, 0.05% Tween 80 (Sigma), and 10% albumin dextrose catalase obtained from Difco Laboratories, USA, at 37 °C for 7–10 days. The cell colony was harvested by carrying out centrifugation then it was washed twice in 7H9 broth again it was suspended in fresh 7H9 broth. Several aliquots of 0.5 ml were dispensed and the seedlots of suspension was stored at –70 °C for further use. To test the viability of prepared culture one of the vial was thawed and plate cultured to determine the colony forming unit (CFU).

Compounds **7a–t** stock solutions were prepared and dilutions were made, all test compound stocks and dilutions were prepared in DMSO. MICs of all test compounds were determined in Middlebrook 7H9 broth by the standard microdilution method described by Marry et al. In a 384 well plate 1 μ l of serial two-fold dilutions of test compound was poured in concentration range of 100 μ M–0.19 μ M. The control wells contained media and culture controls only; Isoniazid was used as standard reference for the assay. As per the reported method, 40 μ l (3–7 \times 10⁵ CFU/ml) of the bacterial culture was added to all the wells. Only the control wells were devoid of culture. The plates were incubated at 37 °C for 5 days packed in gas permeable polythene bags. After the completion of incubation period, each well was introduced with a freshly prepared 1:1 mixture of Resazurin (0.02% in water), and 10% Tween 80 with 8 μ l in quantity. It is understood that change in colour indicates growth or inhibition, if the colour of solution in well changes to blue then it is assumed as inhibition and if changes to pink then growth of the culture. To determine this change all the plates were again incubated for 24 h at 37 °C and then the change in each well was observed.

A concentration at which change of colour from blue to pink in

inhibited shall be considered as the minimum inhibitory concentration (MIC). Solutions from all the wells were studied for their absorbance at 575 nm and 610 nm then ratio was calculated, an 80% inhibition was considered as MIC. The minimum bactericidal concentration (MBC) is the lowest concentration of an antibacterial agent required to kill the bacteria under study. Aliquots from sample wells (MIC and higher) from the MIC plates were diluted 1:10 and subcultured on 7H10 agar plates. These were incubated at 37 °C for 3–4 weeks (without test compounds), CFU was studied. The lowest concentration of test compound that resulted in a reduction of about two log₁₀ CFU from the initial unit was considered as MBC [26].

4.2.2. DprE1 activity and inhibition studies

Liav A. et al. [27] described a simple method for the synthesis of β-D-ribofuranose (FPR), it was obtained following the reported method and employed as substrate for the evaluation of enzyme activity of DprE1 along with 2,6-dichlorophenolindophenol (DCPIP). The test assay was carried out on a UV–visible spectrophotometer at a constant temperature of 25 °C for recording the decrease in absorbance at 600 nm. DprE1 (3 μM) was incubated for 7 min with 100 μM FPR in the presence of different inhibitor concentrations (0–100 μM for **7a**, **7e**, **7f**, **7o**; all inhibitors were dissolved in 100% DMSO with constant concentration. Then the enzyme activity was measured using the DCPIP assay with a final protein concentration of 0.3 μM. The IC₅₀ values were obtained by plotting the initial velocities with the following equation

$$A_{[I]} = A_{[0]} \times (1 - [I]/[I] + IC_{50})$$

where,

$A_{[I]}$ is the enzyme activity at inhibitor concentration [I] and $A_{[0]}$ is the enzyme activity in absence of inhibitor.

4.3. In vivo studies

Ethics statement and animals

All animal experiment protocols and usage was approved by Institutional Animal Ethics Committee (IAEC) at the Department of Pharmaceutical Sciences, Rashtrasant Tukadoji Maharaj Nagpur University, Nagpur, registered with the Committee for the Purpose of Control and Supervision of Experiments on Animals (CPCSEA), Government of India. All rats were housed in a temperature and humidity controlled room with 12-h light/dark cycle. All rats were allowed free access to regular food and tap water.

4.3.1. Physicochemical studies

The physicochemical properties (Log P) of compounds **7a**, **7e**, **7f** and **7o** were determined following method described by Takics-Novfik and Avdeef (Shake Flask method). To a 10 mM sodium phosphate buffer of pH 7.4 in water was added 10 mM of test compound solution prepared in DMSO. The DMSO was removed from solution and to it 400 μl of octanol was added and then it was shaken for 5 h at 25 °C. The solution was then centrifuged for 30 min at 3000 RPM using cooling centrifuge. An UV–HPLC analysis was carried out to quantify the aqueous layer and the octanol layers to calculate Log D value. Following formula was applied to determine values; $\text{Log } P = \text{Log} (\text{Octanol}/\text{Octanol inj volume})/(\text{Buffer}/\text{Buffer inj volume})$.

4.3.2. Pharmacokinetic studies

The pharmacokinetic properties were investigated following the procedure reported by Gao et al. Six groups consisting of six animals per group of Sprague Dawley rats weighing 180–220 g were used in the study. The rats were fasted overnight before starting the

test protocol. Four of the six groups were administered with compounds **7a**, **7e**, **7f** and **7o** at 10 mg/kg (*i.v.*), and 20 mg/kg (*p.o.*). Blood was collected from the jugular vein of each test and control animal at time frequency of 2, 5, 10, 15, 30 and 45 min and 1, 2, 4, 6, 8, 12 and 24 h after a single *i.v.* dosing. After 15, 30, 45 min and 1, 1.5, 2, 3, 4, 6, 8, 12 and 24 h for single oral dose. All blood samples were subjected to centrifugation at 3000 RPM for 10 min. The separated serum was then stored at –20 °C for subsequent studies. 100 μl of the serum was extracted with about 500 μl of acetonitrile and then the organic layer was dried. Dried sample was reconstituted with acetonitrile for HPLC analysis. The peak concentration (C_{max}), the time to reach peak concentration (T_{max}), the elimination half-time ($t_{1/2}$) and the total area under the concentration time curve (AUC) of compounds **7a**, **7e**, **7f** and **7o** was determined from the HPLC data and statistical analysis [24,25].

4.4. Single crystal X-ray studies

X-ray data for compound **7a** was collected on a BRUKER-AXS SMART APEX CCD X-ray diffractometer, using graphite-monochromatic Mo K α radiation (= 0.71073 Å). Data was reduced using SAINTPLUS [27], and a multi-scan absorption correction using SADABS [28] was performed. The structure was solved using SHELXS-97 and full matrix least-squares refinements against F² were carried out using SHELXL-97 [29,30]. All ring hydrogen atoms were assigned on the basis of geometrical considerations and were allowed to ride upon the respective carbon atoms. All hydrogen atoms were assigned fixed U_{iso} values, equal to 1.2U_{eq} of the parent atom for ring and 1.5U_{eq} for methyl hydrogen. Crystallographic data and structure refinement parameters are presented in Table 3 for compounds **7a**, the CCDC deposition number for **7a** is CCDC 1041108.

4.5. Molecular docking

For docking purpose, the three-dimensional structure of DprE1 (PDB code: 4KW5) was obtained from RCSB protein Data Bank. The receptor molecule was refined and validated on the basis of Ramchandran plot using Biopredicta© module on the Vlife MDS Molecular Modelling Software, Version 4.3.1 [31]. Ligands that were already present within the receptor in bound form were removed but the FAD molecule was retained intentionally to allow for docking protocol. All the ligands were prepared and docked for this study in flexible docking mode and atoms located within a range of 5.0 Å from the amino acid residues were selected in the active site. The docking calculations and energy minimization were set in the Biopredicta© module, most of the parameters were set default with 10,000 cycles per molecule for the active site cavity no. 1. This cavity consisted of amino acid residues Lys134, Tyr314, Ser228, Lys367, Asn385, Gln336, His132, Val365, Gln334, Cys387, Tyr60, Lys418 and external residue Flavin (FAD). This cavity was selected on the basis of reported crystal structure of lead molecule ethyl (2-[(1, 3-benzothiazol-2-yl) carbonyl] amino] thiophen-3-yl) carbonyl carbamate (TCA1) [32–34].

4.6. Three dimensional quantitative structure activity relationship studies using k-nearest neighbour molecular field analysis (kNN-MFA 3D QSAR) method

Three-dimensional structures were drawn for each molecule in ChemDraw molecular design suite and the geometries were optimized using Monte Carlo conformational analysis, Merck Molecular Force Fields (MMFF) and other charges in the Vlife MDS engine 4.3.1 [35,36]. The Vlife MDS engine consist of the 2D and 3D studies, we selected the 3D studies to explain QSAR for the newly synthesized

compounds. The molecules were aligned by the template based techniques using the basic nucleus. 3D descriptors such as Tripos force field, electrostatic, steric and hydrophobic field types, with cut-off values of 10.0 and 30.0 kcal/mol respectively with Gasteiger and Marsilli charge type was selected for building the model, about 5100 field descriptors were studied and analysed. As the model is based on grid based method a rectangular grid was formed initially around the molecules.

The set of molecules was divided into training and test set based on the sphere exclusion method leading to a training set of 14 molecules and test set of 6 molecules. In pursuit of better model we studied all the three possible methods based on the *k*NN-MFA namely *k*-Nearest Neighbour-Stepwise Variable Selection, *k*-Nearest Neighbour-Genetic Algorithm, *k*-Nearest Neighbour-Simulated Annealing. The descriptors were obtained in form of field points and correlation plots for all the molecules.

4.7. Pharmacophore modelling

Pharmacophore modelling for the series was carried out on selected molecules with better biological activity. Compounds **7a**, **7e**, **7f** and **7o** with better biological activity were first aligned to build a pharmacophore model. Molesign module was set to generate minimum four pharmacophore features necessary for the bioactivity of ligand, the tolerance limit and maximum distance between two features was limited to 10 units and 10 Å respectively for identification of pharmacophore. The average root mean square deviation (RMSD) between alignments of pharmacophore alignments of molecules was restricted to 0.055.

5. Results and discussion

5.1. Chemistry

The synthetic route used for obtaining designed compounds is outlined in Scheme 1.

5.1.1. Synthesis of compounds 1–4

Aniline **1** in presence of hydrochloric acid reacts with potassium thiocyanate to yield phenyl thiourea **2** in good yield. Phenyl thiourea undergoes cyclisation in presence of bromine at 0–5 °C to provide with 2-aminobenzothiazole **3**. The reactions and product details are not mentioned in the manuscript as these are reported earlier. 2-Aminobenzothiazole was reacted with ethyl acetoacetate in presence of sodium hydroxide at 120 °C in toluene to yield benzothiazolyl oxobutanamide **4** in high yield of 88% in around 18 h based on the TLC monitoring of reaction progress. Spectroscopic studies establish the structure of **4**, the IR spectrum showed absorption bands at 3343.58 cm⁻¹ and 1292.22 cm⁻¹ indicating the presence of the N–H and C–N of amide respectively, it also presented with the C=O at 1690 cm⁻¹ for the ester character of compound. ¹H NMR study displays the aliphatic protons at δ 2.25 and 3.66 corresponding to the singlets for methyl and ethyl protons in the chain, protons between δ 7.53 and 8.03 belongs to aromatic ring of benzothiazole, the amide proton was found the upfield at δ 12.49. The ¹³C NMR studies indicate the aliphatic and aromatic carbons in between δ 29 to 51 and δ 118 to 202 respectively. The compound was finally confirmed on by mass analysis and found to be 234.27 with M⁺H at about 235.04.

5.1.2. Synthesis of compound 7a–t

Cyclocondensation of benzothiazolyl oxobutanamide **4** with various substituted aryl aldehydes **5** and thiourea **6** in presence of *p*-toulene sulfonic acid (*p*TsOH) yield the titled compounds **7a–t** (Scheme 1). This reaction was carried out in methanol at reflux

temperature for about 12 h, it follows the classical three component one pot Biginelli reaction mechanism and yield products in medium to good yield. All the derivatives were extracted and recrystallized from DMF to give yield between 60 and 75 %.

All the 20 derivatives were analysed on the basis of spectral and elemental analysis. The IR spectra data of derivatives exhibit absorption bands at 3112 cm⁻¹ (N–H str), 2926 cm⁻¹ (methyl, C–H str-asy) and 2853 cm⁻¹ (C–H str-sym) for the formed pyrimidine nucleus. The bands 1671 cm⁻¹ (amide C=O) and 1505 cm⁻¹ (C–N str) presents the amide side chain continuing to the benzothiazole portion of the molecule. The ¹H NMR spectra of this series exhibits common peaks for the methyl group around δ 2.6 as singlet which indicates methyl group attached to pyrimidine ring. Two amide protons around 4.3 ppm and broad singlet and a distant amide proton above 8.5 ppm exhibit the presence of amide group on the aromatic and aliphatic parts of the molecules. A singlet exhibiting one proton supports 1,2,3,4 tetrahydro nature of pyrimidine ring further supporting structure elucidation. The ¹³C NMR of synthesised derivatives shows the distant aliphatic and aromatic carbon nucleus, prominent aliphatic nuclei were exhibited around 14.0 and 55.7 corresponding to the methyl and the amide groups. Other nuclei belong to the aromatic region from 106 to 201 ppm exhibiting aromatic nature of the molecule. The structure of all the derivatives were finally confirmed by ESI-MS studies and were found to be correct based on the M+H and M–H peaks on the mass spectrums.

5.2. Biological evaluation

5.2.1. In vitro anti-tubercular studies for determination of minimum inhibitory concentration (MIC) and minimal bactericidal concentration (MBC)

The *in vitro* studies were carried out on virulent strain of *M. tuberculosis* H₃₇Rv (ATCC 27294) to determine MIC of test compounds with Isoniazid as standard reference. Microbial culture was developed on Middlebrook 7H9 broth supplemented with 0.2% glycerol, 0.05% Tween 80 (Sigma), and 10% albumin dextrose catalase. The method for testing was based on the protocols and modifications reported by Jayaram et al. and Marry et al., these methods were found to be more suitable and useful in case of Mtb. The test compounds were prepared as stock and dilutions in DMSO and MIC was determined by microdilution technique, which was evaluated further for the determination of the CFU. After the incubation period of culture in presence or absence of test compounds, the viability of bacteria was determined by observing the colour change from blue to pink of Resazurin mixture which acts as indicator of the inhibitory activity and potency. It was found that compounds **7a**, **7e**, **7f** and **7o** exhibited MIC between 0.08 and 0.09 μM which is found to be better than the standard reference Isoniazid with MIC of 0.2 μM. These results are found to be exiting since the lead molecule TCA1 has shown the MIC of 0.19 μM (Table 1). The compounds with good MIC were found to be substituted with halogens like fluorine, chlorine and bromine which are good dual acting substitutions causing an electron withdrawing nature on the ring nucleus. Earlier it was reported that NO₂ group containing compounds are inhibiting the DprE1 selectively due to conversion of the nitro to amino moiety by its interaction with amino acid Cys387. In case of the lead moiety TCA1 it was found to be interacting with residues Cys387 and Tyr314 noncovalently but this molecule dose not bear any nitro substitution. This encouraged us further to determine the DprE1 selectivity of our test compounds.

5.2.2. DprE1 activity and inhibition studies

This enzymatic assay was carried out on the selected

Table 1

Data of the *in vitro* studies for MIC for *M. tuberculosis* (H₃₇Rv), IC₅₀ for DprE1 inhibition study and ClogP by the Shake-Flask method.

Sr. No.	Compd	R	MIC ^a (μM) H ₃₇ Rv	IC ₅₀ ^b (μM) DprE1	ClogP ^c	ClogP ^d
1	7a	H	0.08	7.7 ± 0.8	2.02	2.03
2	7b	2-Cl	0.32	NT ^e	2.49	NT
3	7c	4-Cl	0.32	NT	2.74	NT
4	7d	2,4-Di Chloro	0.25	NT	3.20	NT
5	7e	4-F	0.09	9.2 ± 1.5	2.17	2.18
6	7f	CF ₃	0.09	11.1 ± 1.8	2.91	2.92
7	7g	4-Br	0.4	NT	2.89	NT
8	7h	2-NO ₂	1.2	NT	1.77	NT
9	7i	3-NO ₂	1.3	NT	1.77	NT
10	7j	4-NO ₂	1.2	NT	1.77	NT
11	7k	2-OMe	0.5	NT	1.42	NT
12	7l	4-OMe	0.5	NT	1.98	NT
13	7m	2-OH	2.4	NT	0.92	NT
14	7n	4-OH	2.4	NT	1.42	NT
15	7o	4-N(CH ₃) ₂	0.08	10.3 ± 2.6	2.23	2.22
16	7p	3-OH-4-OMe	1.2	NT	1.24	NT
17	7q	2-OH-3-OMe	1.4	NT	0.74	NT
18	7r	4-OH-3,5-Di OMe	1.2	NT	1.0	NT
19	7s	4-CH ₃ CO ₂	3.1	NT	1.41	NT
20	7t	4-C ₆ H ₅ CH ₂ O	1.6	NT	3.74	NT
21	INH ^f	—	0.2	—	—	—

^a Minimum inhibitory concentration against *M. tuberculosis* (Mtb) H₃₇Rv ATCC 27294.

^b IC₅₀ determined from DprE1 Activity and inhibition studies.

^c Calculated for CambridgeSoft corporation's ChemDraw Ultra 11.0.

^d Determined by Shake-Flask method with HPLC.

^e Not tested.

^f Isoniazid.

compounds which have shown good MIC in the cell cultures. The UV-spectrophotometric method for 2,6-dichlorophenolindophenol (DCPIP) and DprE1 activity assay was carried out on the β-D-ribofuranose (FPR) substrate as described earlier by Liav A. et al. the mixture was incubated for 7 min at different concentrations of test compounds **7a**, **7e**, **7f** and **7o**. The inhibition concentration and enzyme activity in absence of inhibitor was determined and reported in Table 1. It was observed that the IC₅₀ for tested compounds was different for all the four compounds which led us to determine the partition coefficient of the molecules showing selectivity towards DprE1. **7a** and **7o** exhibited IC₅₀ of 7.7 ± 0.8 μM and 10.3 ± 2.6 μM respectively, whereas the fluoro derivatives had varied IC₅₀ of 9.2 ± 1.5 and 11.1 ± 1.8 for *p*-F and *p*-CF₃ substituted derivative respectively.

5.2.3. Physicochemical studies

Selected compounds from this series were subjected to determination of their partition coefficient (Log *P*), this was carried out by the shake-flask method developed by Takics-Novfik and Avdeef.

Table 2

Study on selected compounds for pharmacokinetic and bioavailability studies.

Sr. No.	Compd	Route	Dose (mg/kg)	C _{max} (μg/ml)	T _{max} (h)	t _{1/2} (h)	AUC _{0-∞} (μg·h/ml)	F ^c (%)
1	7a	<i>i.v.</i> ^a	10	1.80	—	2.6	1.50	—
		<i>p.o.</i> ^b	20	0.59	0.5	5.5	0.79	52.66
2	7e	<i>i.v.</i>	10	1.50	—	2.8	1.53	—
		<i>p.o.</i>	20	0.34	0.6	5.8	0.81	51.92
3	7f	<i>i.v.</i>	10	1.73	—	2.6	1.64	—
		<i>p.o.</i>	20	0.49	0.6	6.0	0.83	50.60
4	7o	<i>i.v.</i>	10	1.62	—	2.5	1.48	—
		<i>p.o.</i>	20	0.41	0.5	5.4	0.78	52.70

^a Intra Venous route.

^b Per Oral route.

^c Oral bioavailability.

In this method the compounds were treated in a binary system of Water: Octanol and the UV-HPLC analysis was carried out to determine the concentration of compounds in each layer after a set time. The results are reported in Table 2 along with theoretical values obtained from computational algorithm. It was found that the computationally determined and practically found ClogP values are in good understanding with each other exhibiting the coefficient of partition around 2.03 to 2.92 which is way below the mark of 5 according to the Lipinski rule of 5 for druglikeness of compounds under test.

5.2.4. Pharmacokinetic studies

The lead compound BTZ043 was reported as selective DprE1 inhibitor but its pharmacokinetic profile was not found to be satisfactory. Further the same series was further exploited by Gao C et al., to improve the pharmacokinetic profile of benzothiazinones. In their report a molecule '8-nitro-2-(1,4-dithia-8-azaspiro[4.5]decan-8-yl)-6-(trifluoromethyl)-4H-benzo[e][1,3]thiazin-4-one (8o)' had exhibited oral bioavailability of 26%, however this was found to be an meagre improvement for infections like tuberculosis as it will not help improve the aim to reduce the dosage frequency in therapy.

We studied the pharmacokinetic profile of selected molecules from our series by determining the peak concentration (C_{max}), the time to reach peak concentration (T_{max}), the elimination half-time (t_{1/2}) and the total area under the concentration time curve (AUC) of compounds **7a**, **7e**, **7f** and **7o** by HPLC study and statistical analysis. Sprague Dawley rats were employed for the study in group of six. Out of which four groups were administered with compounds **7a**, **7e**, **7f** and **7o** at 10 mg/kg (*i.v.*), and 20 mg/kg (*p.o.*). Blood was collected at time interval of 2, 5, 10, 15, 30 and 45 min and 1, 2, 4, 6, 8, 12 and 24 h after a single *i.v.* dosing. After 15, 30, 45 min and 1, 1.5, 2, 3, 4, 6, 8, 12 and 24 h for single oral dose. It was found that the compound **7a** had bioavailability of 52.66% per orally with C_{max} of 0.59 and 1.80 for *p.o.* and *i.v.* dose respectively. The T_{max} and t_{1/2} were found to be 0.5 and 5.5 h respectively. This was found to be similar for other three compounds as well (Table 2) with **7o** exhibiting slight more % bioavailability than **7a** possibly owing to presence of dimethyl amino groups on the phenyl ring as substitution.

5.3. Single crystal X-ray studies

One of the potent compounds for the series **7a** was selected for this study owing to its crystalline nature and formation of triclinic crystal morphology. The X-ray data was collected on a BRUKER-AXS SMART APEX CCD X-ray diffractometer, using graphite-monochromatic Mo K_α radiation (= 0.71073 Å). Data was reduced and multi-scan absorption correction was carried out using SAINTPLUS and SADABS respectively. The structure was solved on SHELXS-97 and full matrix least-squares refinements against F² were carried out using SHELXL-97. The data for crystal structure is detailed in Table 3, the compound crystallizes in a triclinic system with space group P1, containing 4 molecules in the unit cell. The labelled ORTEP diagram of **7a** is exhibited in Fig. 3(a) and (b) depicting the molecular structure in two different views at 30% probability. The asymmetric unit of **7a** contains structurally almost identical and crystallographically independent dimerically hydrogen bonded two molecules as shown in Fig. 4 where the hydrogen are removed intentionally for purpose of clarity. The selected bond distances and bond angles of the compound **7a** are listed in Table 4.

Table 3
Crystallographic data and structure refinement for compound **7a**.

Parameters	<i>N</i> -(1,3-benzothiazol-2-yl)-6-methyl-4-phenyl-2-thioxo-1,2-dihydropyrimidine-5-carboxamide 7a
Formula	C ₁₉ H ₁₆ N ₄ OS ₂
Formula weight	380.48
Crystal system	Triclinic
<i>a</i> (Å)	8.5549(13)
<i>b</i> (Å)	14.176(2)
<i>c</i> (Å)	16.102(3)
α (°)	70.945(2)
β (°)	77.271(2)
γ (°)	82.569(2)
<i>V</i> (Å ³)	1796.9(5)
<i>Z</i>	4
space group	<i>P</i> 1
<i>T</i> (K)	298(2)
Crystal size (mm ³)	0.40 × 0.36 × 0.30
ρ_{calcd} (g cm ⁻³)	1.406
μ (mm ⁻¹)	0.312
θ Range (°)	1.363 to 26.106
<i>h</i> / <i>k</i> / <i>l</i> indices	−10, 10/−17, 17/−19, 19
Reflections collected	18736
Uniquereflect, [<i>R</i> _{int}]	7059, 0.0247
GOOF	1.030
<i>R</i> 1[<i>I</i> > 2(σ <i>I</i>)]	0.0407
<i>wR</i> 2[all data]	0.1177

5.4. Molecular docking studies

The molecular docking study was carried out to explore binding modes of our derivatives with the DprE1 enzyme. The molecular

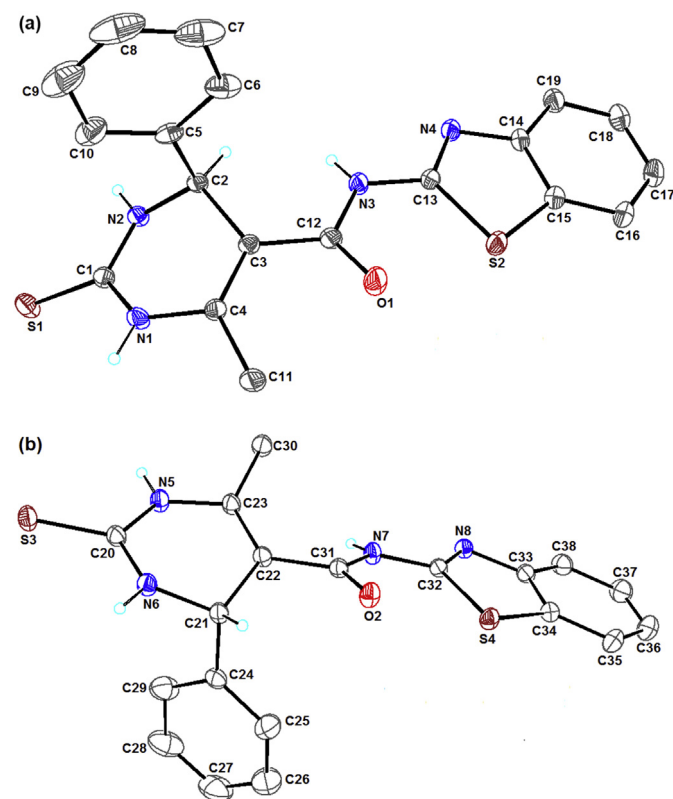


Fig. 3. (a) and (b) are the ORTEP views of **7a**. Hydrogen atoms on the aromatic ring of the molecule are omitted for clarity. The thermal ellipsoids are represented at the 30% probability level. Colour code for atoms: Grey, C; Cyan, H; Blue, N; Red, O; Brown, S. (For interpretation of the references to colour in this figure legend, the reader is referred to the web version of this article.)

docking simulation studies were carried out by Biopredicta tool of VLife MDS software version 4.2. On the basis of *in vitro* studies and DprE1 selective inhibitory action of molecules were selected for this study. The receptor employed here was DprE1 (PDB code: 4KW5) obtained from RCSB Protein Data Bank (RCSB-PDB). The initial crystal structure consisted of the bound ligand, it was removed and the missing loops were added with the help of homology modeling module from the same software. For our purpose the lead molecule was TCA1 which consisted of the benzothiazole nucleus, so the cavity for this reference molecule was selected for carrying out the docking of selected derivatives. The interacting amino acid residues were identified as Lys134, Tyr314, Ser228, Lys367, Asn385, Gln336, His132, Val365, Gln334, Cys387, Tyr60, Lys418 external residue Flavin (FAD) and the ligand molecule.

The binding modes of all the four selected compounds are presented in Fig. 5a–d. It exhibits that these molecules show interactions with the major residues like Cys387 and Tyr314 forming noncovalent interactions with these. The compound **7a** forms overlapping hydrophobic bonds with cys387 and the methyl group of the pyrimidine ring, it all forms the van der Waals interaction with pyrimidine ring nitrogen. These molecules show about 13–15

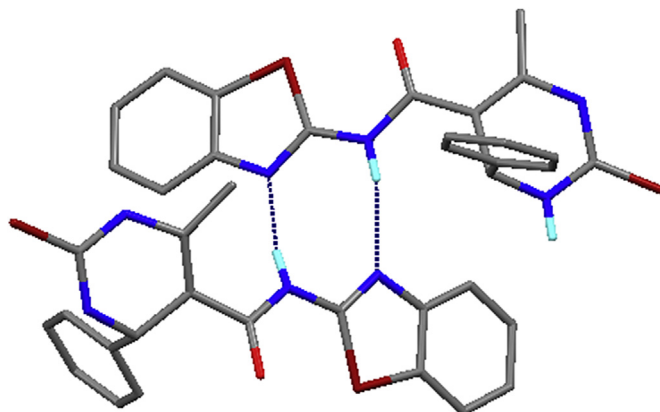


Fig. 4. Hydrogen bonded dimeric view of compound **7a**.

Table 4
Selected bond distances (Å) for compound **7a** based on crystallographic data.

S(1)–C(1)	1.6755(18)	S(2)–C(15)	1.745(2)	S(2)–C(13)	1.7469(17)
S(3)–C(20)	1.6866(18)	S(4)–C(34)	1.7359(19)	S(4)–C(32)	1.7383(16)
O(1)–C(12)	1.216(2)	O(2)–C(31)	1.218(2)	N(3)–C(13)	1.380(2)
N(1)–C(1)	1.365(2)	N(2)–C(1)	1.329(2)	N(3)–C(12)	1.384(2)
N(1)–C(4)	1.387(2)	N(2)–C(2)	1.459(2)	N(4)–C(13)	1.293(2)
N(4)–C(14)	1.388(2)	N(5)–C(20)	1.352(2)	N(5)–C(23)	1.395(2)
N(6)–C(20)	1.321(2)	N(6)–C(21)	1.462(2)	N(7)–C(31)	1.366(2)
N(7)–C(32)	1.381(2)	N(8)–C(32)	1.296(2)	N(8)–C(33)	1.392(2)

interaction with these residues, however for visibility and clarity only selected bonds are exhibited. Compound **7e** forms hydrogen bonds with the nitrogen proton of pyrimidine nucleus Asn385, Cys387 forms a van der Waals interaction, Tyr16 forms a pi interaction with benzothiazole moiety, whereas an hydrophobic interactions are seen between Cys387 residue. Compound **7f** exhibits noncovalent interactions within the cavity, it forms hydrogen bond between pyrimidine and Gly117, Hydrophobic interaction between the fluoro group and Cys387 and Gly336, van der waals interaction between the benzothiazole moiety and the Lys418 and Val365. **7o** interacts within the selected cavity exhibiting all the four types of bindings, pyrimidine ring forms hydrogen bond and van der Waal interaction with the His132 amino acid, benzothiazole nucleus forms a pi interaction with the Trp15 and FAD514.

The substitution on aromatic ring forms extensive interaction with the Cys387, Val365, Gly336 of hydrophobic and van der Waal forces (see Fig. 6).

Interactions produced by these molecules are similar to the lead molecule TCA1, this directs that a substitution on the pyrimidine ring has contributed towards increased potency to the DprE1 selectivity and further substitution on the pyrimidine ring can produce molecules with enhanced selectivity leading to development of the lead molecules for this series forming potent antitubercular agents.

5.5. Interpretation of 3D QSAR model generated by kNN-MFA method

The 3D QSAR model for newly synthesized series of molecules was generated on VLife MDS 3D QSAR module by kNN-MFA method and three different algorithms were applied namely; Stepwise Variable Selection (SWV), Genetic Algorithm (GA) and Simulated Annealing (SA). The SWV method optimizes the nearest neighbour (k) and selections of variables are made for the original pool of set. GA method mimics the process of natural selection and most suitable of the molecule is given preference, in case of the SA method simulation of a physical process involving the annealing process leading to distortion and regaining of the confirmation is involved.

In present study all three methods were applied to build QSAR model, Table 5 exhibits the predicted values and residuals obtained from the study. It was found that the third model 'Model C' obtained from kNN-SA method was found to be best suited for this series of compounds based on comparative statistical coefficients with other models like q^2 (0.50), q^2_{se} (0.64), $pred_r^2se$ (1.00). The

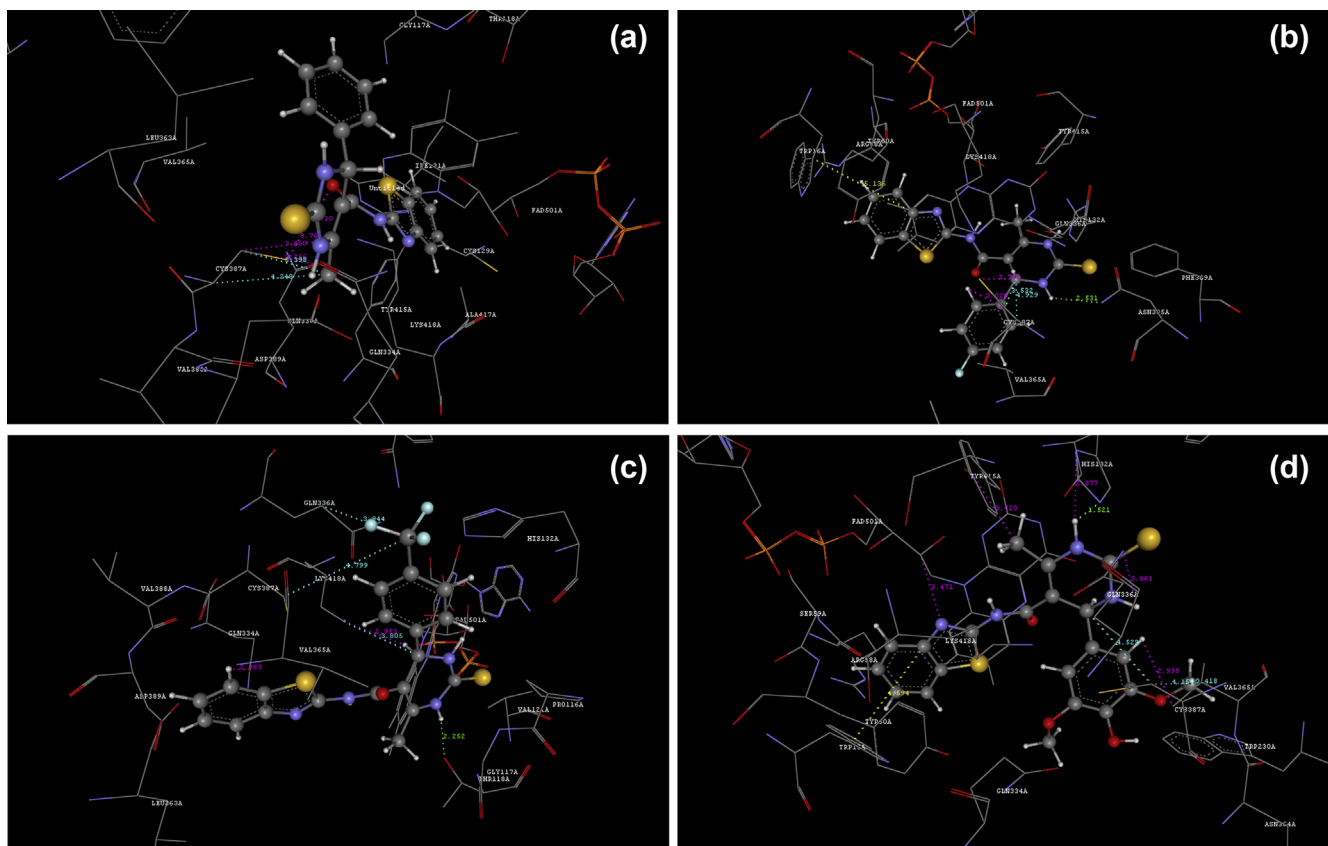


Fig. 5. Binding model of compounds **7a**, **7e**, **7f** and **7o** with DprE1 target cavity. The green, blue, yellow and magenta colour dashed lines represents Hydrogen bonds, hydrophobic interactions, pi interactions and van der Waals forces respectively. (For interpretation of the references to colour in this figure legend, the reader is referred to the web version of this article.)

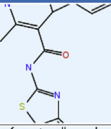
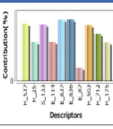
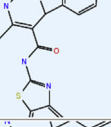
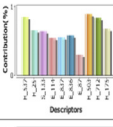
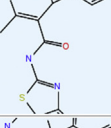
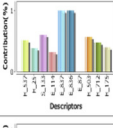
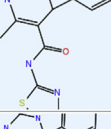
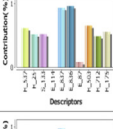
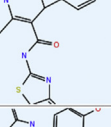
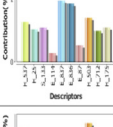
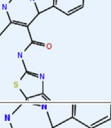
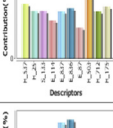
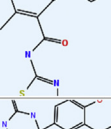
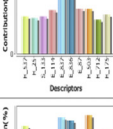
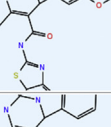
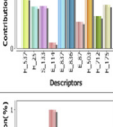
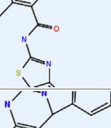
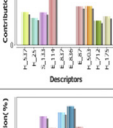
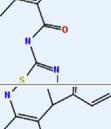
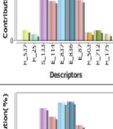
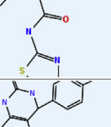
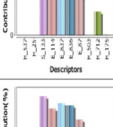
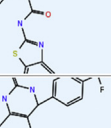
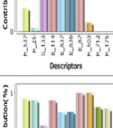
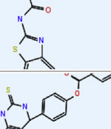
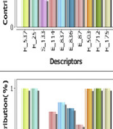
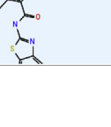
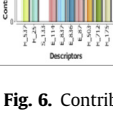
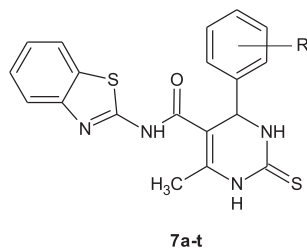
	Molecule	Graph	H_537	H_25	S_133	E_114	E_837	E_836	E_87	H_503	H_175	H_175
1			0.271	0.225	-0.002	0.702	-0.381	-0.313	0.651	0.527	0.37	0.326
2			0.325	0.262	-0.002	0.811	-1.077	-0.783	0.869	0.658	0.577	0.374
3			0.232	0.216	-0.002	0.57	1.028	0.837	0.436	0.492	0.329	0.318
4			0.261	0.239	-0.002	0.219	0.745	0.709	0.56	0.537	0.338	0.351
5			0.265	0.238	-0.002	0.372	0.899	0.55	0.815	0.559	0.339	0.348
6			0.251	0.237	-0.002	0.662	-1.316	-0.954	0.911	0.536	0.347	0.35
7			0.221	0.228	-0.003	0.826	-0.175	-0.01	1.261	0.494	0.3	0.339
8			0.244	0.229	-0.003	0.293	-0.606	-0.63	0.862	0.548	0.246	0.335
9			0.238	0.225	-0.002	1.301	-3.725	-3.049	1.341	0.525	0.272	0.332
10			0.115	0.16	-0.002	0.644	-1.116	-0.681	1.013	0.238	0.066	0.251
11			0.086	0.149	-0.002	0.708	-0.914	-0.724	0.966	0.196	0.155	0.239
12			0.146	0.154	-0.002	0.707	-1.351	-1.189	0.935	0.239	-0.005	0.238
13			0.341	0.3	-0.003	1.168	-0.481	-0.36	1.863	0.713	0.527	0.387
14			0.368	0.321	-0.005	0.891	-0.049	-0.421	1.024	0.711	0.69	0.439

Fig. 6. Contribution plot for 3D-QSAR SA kNN MFA method of Model C for series 7a–t.

Table 5
3D QSAR data by the k-Nearest Neighbour (kNN) method for **7a–t**.



Sr. No.	R	Model A			Model B			Model C		
		3D QSAR by SWV-kNN MFA ^d			3D QSAR by GA-kNN MFA ^e			3D QSAR by SA-kNN MFA ^f		
		Obs. Act ^b	Pre. Act ^c	Res ^g	Obs. Act	Pre. Act	Res	Obs. Act	Pre. Act	Res
1	H	1.09691	1.09691	0	1.09691	-0.38021	1.47712	1.09691	1.09691	0
2	2-Cl	0.49485	-0.38021	0.87506	0.49485	0.39794	0.09691	0.49485	0.39794	0.09691
3	4-Cl	0.49485	1.09691	-0.60206	0.49485	0.39794	0.09691	0.49485	0.39794	0.09691
4	2,4-Di Chloro	0.60205	-0.11394	0.71599	0.60205	1.0457	-0.44365	0.60205	0.39794	0.20411
5	4-F	1.04575	-0.20411	1.24986	1.04575	-0.49136	1.53711	1.04575	-0.49136	1.53711
6	CF ₃	1.04575	-0.11394	1.15969	1.04575	-0.49136	1.53711	1.04575	-0.14612	1.19187
7	4-Br	0.39794	1.09691	-0.69897	0.39794	0.30102	0.09692	0.39794	-0.49136	0.8893
8 ^a	2-NO ₂	-0.07918	-0.11394	0.03476	-0.07918	-0.11394	0.03476	-0.07918	-0.11394	0.03476
9	3-NO ₂	-0.11394	-0.38021	0.26627	-0.11394	-0.11394	0	-0.11394	-0.11394	0
10 ^a	4-NO ₂	-0.07918	-0.07918	0	-0.07918	0.30102	-0.3802	-0.07918	-0.49136	0.41218
11 ^a	2-Ome	0.30102	-0.07918	0.3802	0.30102	0.30102	0	0.30102	0.30102	0
12	4-Ome	0.30102	-0.49136	0.79238	0.30102	0.30102	0	0.30102	0.30102	0
13	2-OH	-0.38021	-0.11394	-0.26627	-0.38021	1.09691	-1.47712	-0.38021	0.30102	-0.68123
14 ^a	4-OH	-0.38021	0.39794	-0.77815	-0.38021	1.09691	-1.47712	-0.38021	1.09691	-1.47712
15	4-N(CH ₃) ₂	1.09691	1.09691	0	1.09691	-0.38021	1.47712	1.09691	1.09691	0
16	3-OH-4-Ome	-0.07918	-0.07918	0	-0.07918	-0.49136	0.41218	-0.07918	-0.07918	0
17	2-OH-3-Ome	-0.14612	-0.07918	-0.06694	-0.14612	-0.07918	-0.06694	-0.14612	-0.20411	0.05799
18 ^a	4-OH-3,5-Di Ome	-0.07918	1.09691	-1.17609	-0.07918	1.09691	-1.17609	-0.07918	1.09691	-1.17609
19	4-CH ₃ CO ₂	-0.49136	0.30102	-0.79238	-0.49136	-0.07918	-0.41218	-0.49136	0.39794	-0.8893
20 ^a	4-C ₆ H ₅ CH ₂ O	-0.20411	1.09691	-1.30102	-0.20411	-0.38021	0.1761	-0.20411	1.09691	-1.30102

^a Test Set molecules.

^b Minimum Inhibitory Concentration.

^c Predicted activity.

^d k-Nearest Neighbour-Stepwise Variable Selection.

^e k-Nearest Neighbour-Genetic Algorithm.

^f k-Nearest Neighbour-Simulated Annealing.

^g Residual.

Table 6
The selected k-Nearest Neighbour Simulated Annealing (SA-kNN MFA) QSAR equation along with statistical parameters employed for selecting the model for **7a–t**.

Model no.	Selected descriptors	k	N	Descriptor range	q ²	q ² _{se}	Pred r ²	Pred_r ² se	Degree of freedom
C	H_537 H_25 S_133 E_114 E_837 E_836 E_87 H_503 H_712 H_175	2	14	H_537 0.0856 to 0.2707 H_25 0.1485 to 0.2252 S_133 -0.0023 to -0.0018 E_114 0.7015 to 0.7081 E_837 -0.9144 to -0.3805 E_836 -0.7244 to -0.3133 E_87 0.6511 to 0.9658 H_503 0.1958 to 0.5265 H_712 0.1552 to 0.3697 H_175 0.2391 to 0.3263	0.5000	0.6404	–	1.0094	3

K = Nearest number.

N = Molecules in the test set.

q² = Cross-validated correlation coefficient.

q²_{se} = Standard error of cross-validated correlation coefficient.

r² = Squared correlation coefficient.

Pred_r² = r² for external test set.

Pred_r²se = Standard error of predicted squared regression.

contributing descriptors for this model are listed in Table 6, it enlist the electrostatic, steric and hydrophobic descriptors spread along as field points, the correlation plot is given in Figs. 7 and 8. The electrostatic fields at E_87 (0.6511–0.9658) and E_114

(0.7015–0.7081) are in positive range towards the benzothiazole and pyrimidine-methyl region of the molecule respectively indicating that positive electrostatic potential is favourable for increase in the activity around these positions (Figs. 7 and 8). The

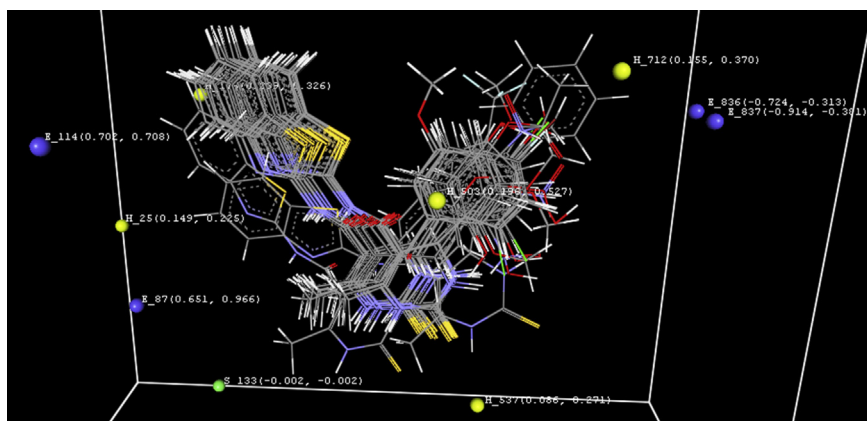


Fig. 7. Field points exhibiting contributing descriptors for 3D-QSAR model C by SA-kNN MFA method for series **7a–t**.

electrostatic lattice point at E_836 (−0.7244 to −0.3133) and E_837 (−0.9144 to −0.3805) around substituted phenyl ring with various substitutions of ‘-R’ is in negative range, it indicates that a negative electrostatic potential is favourable for increase in the activity which suggest that more electronegative substitution will enhance the activity.

The hydrophobic descriptor H_25 (0.149–0.225) in positive range and suggest that an increase in hydrophobic character in this region of amide link contributes towards the activity similarly H_175 (0.2391–0.3263) towards the backdrop of benzothiazole moiety suggests that hydrophobicity contributes in activity which also intuit for a similar substitution on the benzene ring of the moiety can help in enhancing the activity. The descriptors H_503 (0.196–0.527) and H_712 (0.155–0.370) are substitution specific to the compounds **7e** and **7o** respectively and supports for their activity profile, substitutions on the phenyl ring in these molecules have contributed towards their better antitubercular activity. The lattice point S_133 (−0.0023 to −0.0018) exhibit for steric field, an negative range indicates that negative steric potential is favourable for increase in the activity which points out for a reduction of

bulkier groups on the pyrimidine nucleus which may help improve the biological activity.

5.6. Pharmacophore model

Pharmacophore model for selected compounds (**7a**, **7e**, **7f** and **7o**) was generated in the molesign module of VLife MDS 4.1.2 software; the results are given in Fig. 9a, b and Table 7. The model was found to contain small and large coloured spheres which indicate all the possible pharmacophoric centres, the large spheres corresponds to actual pharmacophoric features as aromatic carbon centre (Yellow), hydrogen bond donor and negative charge centre (Green), aliphatic carbon centre (Orange). The distances between all these were found to be within 10 Å and RMSD 0.055 which reveals that the aromatic carbon, hydrogen bond donors and aliphatic groups are the common features necessary for the activity exhibited by derivatives of this series of molecules. The pharmacophore model developed suggests for a DprE1 inhibitor with features like aromatic and aliphatic carbon centres and a negative charge centre is necessary for the activity.

6. Conclusion

In this article we have reported a series of *N*-(1,3-benzothiazol-2-yl)-6-methyl-4-substituted phenyl-2-thioxo-1,2-dihydropyrimidine-5-carboxamide derivatives **7a–t**. These molecules were tested for their antitubercular activity on the virulent strain of *M. tuberculosis* and further the selectivity of these molecules to inhibit DprE1 enzyme was enumerated. Four of the compounds **7a**, **7e**, **7f** and **7o** showed selectivity towards DprE1 and these were further studied for their pharmacokinetic studies. These compounds were also analysed for their docking modes and found to be in comparison with the reference molecules TCA1 and BTZ043. It was summarized that compound **7a** and **7o** have exhibited comparative to better activity with respect to MIC, IC₅₀ and oral bioavailability as well. The molecular docking study revealed that further modification is also possible in the series of molecules to develop into better compounds. The 3D QSAR model suggest for SA method as most suitable statistical algorithm for evaluation of molecules as DprE1 inhibitors with aromatic, aliphatic carbon centres and a negative charge centre as necessary pharmacophoric groups. The future scope for this series lies in testing it for animal studies in various mice models for TB.

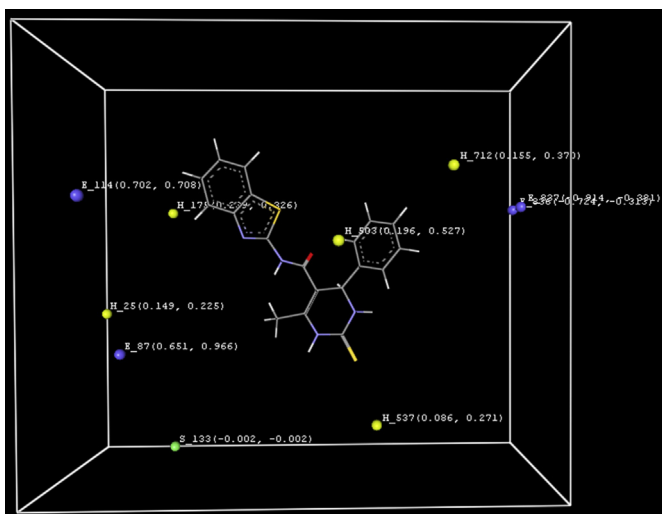


Fig. 8. Field points exhibiting contributing descriptors for 3D-QSAR model C by SA-kNN MFA method for series **7a–t**, figure enumerates the basic nucleus and the descriptor coordinates in the grid.

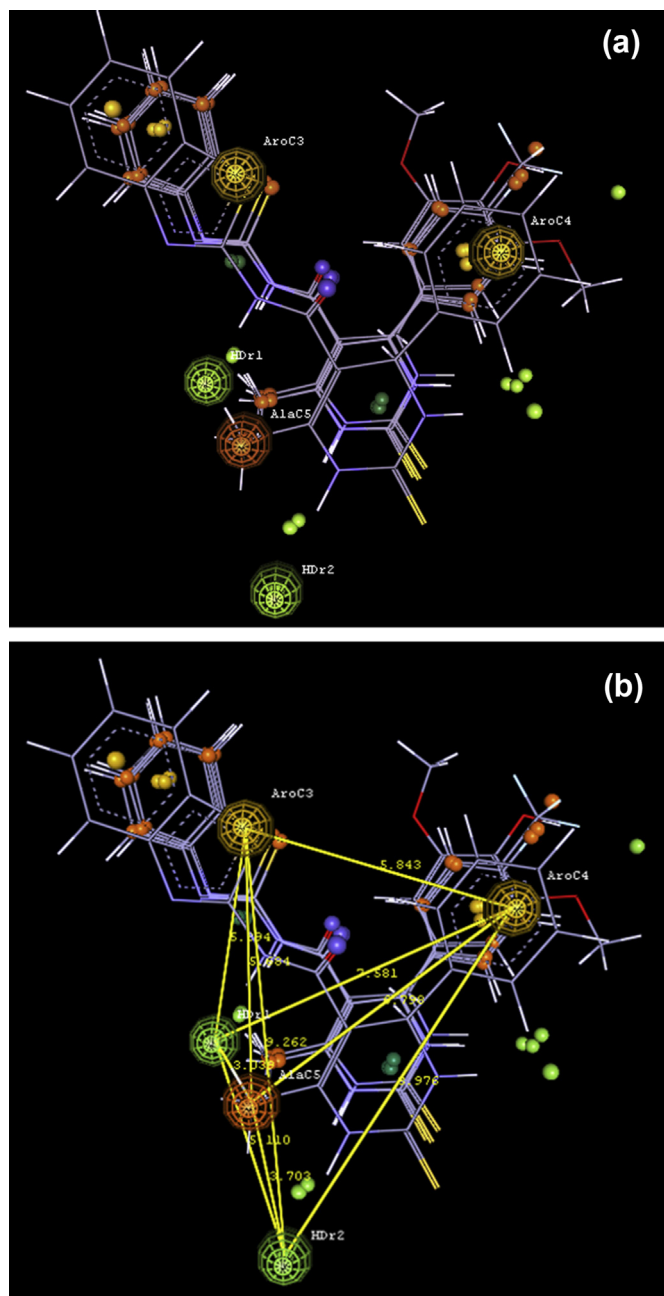


Fig. 9. a. Pharmacophore hypothesis for **7a**, **7e**, **7f** and **7o** exhibiting pharmacophore features as field points for Aromatic carbon centre (Yellow), Hydrogen bond donor and negative charge centre (Green), Aliphatic carbon centre (Orange) as common features revealing that aromatic and hydrogen bond donor groups are important for the activity. b. Pharmacophore identification study with distance between the field points within limit of 10 Å. All the distances are recorded in Table 7. The lines connecting two features are actual distance between the pharmacophores in three dimension field. (For interpretation of the references to colour in this figure legend, the reader is referred to the web version of this article.)

6.1. Crystallographic data

The crystallographic data (excluding structure factors) for the structures in this paper have been deposited with the Cambridge Crystallographic Data Centre with deposition no. CCDC 1041108. Copies of the data can be obtained, free of charge, on application to CCDC, 12 Union Road, Cambridge CB2 1EZ, UK, (fax: +44-(0)1223-336033 or e-mail: deposit@ccdc.cam.ac.uk).

Table 7
Results of pharmacophore identification studies.

Sr. No.	Pharmacophore features (biophores)	Distance (Å)	Sr. No.	Pharmacophore features (biophores)	Distance (Å)
1	AroC3-AroC4	5.843	6	HDr2-HDr1	5.110
2	AroC4-HDr2	8.976	7	HDr1-AlaC5	3.039
3	AroC4-AlaC5	6.798	8	HDr1-AroC3	5.394
4	AroC4-HDr1	7.581	9	AlaC5-AroC3	5.684
5	HDr2-AlaC	3.703	10	AroC3-HDr2	9.262

Acknowledgements

RVC is thankful to Council of Scientific and Industrial Research (CSIR) New Delhi, India for providing financial support in form of SRF: 09/128/0080/2011/EMR-I. PBK acknowledges financial support by University Grants Commission (UGC) New Delhi, India in form of Major Research Project 41-744/2012 (SR). PBK also thanks the Commonwealth Scholarship Commission (CSC), UK for Commonwealth Academic Fellowship INCF-2014-107 for the year 2014-15. RVC also acknowledges the support from SAIIF, Punjab University, Chandigarh for providing spectral data.

Appendix A. Supplementary data

Supplementary data related to this article can be found at <http://dx.doi.org/10.1016/j.ejmech.2015.04.011>.

References

- [1] World Health Organization's 'Global Tuberculosis Report 2014', 11, 2014, pp. 1–14. www.who.int/tb/publications/global_report/gtbr14 (Retrieved on 02 December).
- [2] World Health Organization's 'The Use of Bedaquiline in the Treatment of Multidrug-resistant Tuberculosis: Interim Policy Guidance', 2013, p. 14. http://apps.who.int/iris/bitstream/10665/84879/1/9789241505482_eng.pdf?ua=10.
- [3] A. Zumla, M. Raviglione, R. Hafner, C. Fordham von Reyn, n–3 fatty acids in patients with multiple cardiovascular risk factors, *N. Engl. J. Med.* 368 (2013) 745.
- [4] J. Caminero, G. Sotgiu, A. Zumla, G. Migliori, Treatment of drug-resistant tuberculosis, *Lancet Infect. Dis.* 10 (2010) 621.
- [5] A. Ribeiro, G. Degiacomi, F. Ewann, S. Buroni, M. Incandela, L. Chiarelli, G. Mori, J. Kim, M. Contreras-Dominguez, Y. Park, S. Han, P. Brodin, G. Valentini, M. Rizzi, G. Riccardi, M. Pasca, Analogous mechanisms of resistance to benzothiazinones and dinitrobenzamides in *Mycobacterium smegmatis*, *PLoS One* 6 (2011) e26675–e26675.
- [6] C. Trefzer, H. Škovićová, S. Buroni, A. Bobovská, S. Nenci, E. Molteni, F. Pojer, M. Pasca, V. Makarov, S. Cole, G. Riccardi, K. Mikušová, K. Johnson, Benzothiazinones are suicide inhibitors of mycobacterial decaprenylphosphoryl-β-D-ribofuranose 2'-oxidase DprE1, *J. Am. Chem. Soc.* 134 (2012) 912.
- [7] J. Neres, F. Pojer, E. Molteni, L. Chiarelli, N. Dhar, S. Boy-Rottger, S. Buroni, E. Fullam, G. Degiacomi, A. Lucarelli, R. Read, G. Zanoni, D. Edmondson, E. Rossi, M. Pasca, J. McKinney, P. Dyson, G. Riccardi, A. Mattevi, S. Cole, C. Binda, Structural basis for benzothiazinone-mediated killing of *Mycobacterium tuberculosis*, *Sci. Transl. Med.* 4 (2012) 150ra121.
- [8] V. Makaroc, B. Lechartier, M. Zhang, J. Neres, A. Sar, S. Raadsen, R. Hartkoom, O. Ryabova, A. Vocat, L. Decostend, N. Widmer, T. Budlin, W. Bitter, K. Andries, F. Pojer, P. Dyson, S. Cole, Towards a new combination therapy for tuberculosis with next generation benzothiazinones, *EMBO Mol. Med.* 6 (2014) 372.
- [9] P. Shirude, R. Shandil, C. Sadler, M. Naik, V. Hosagrahara, S. Hameed, V. Shinde, C. Bathula, V. Abadkar, N. Kumar, J. Reddy, V. Panduga, S. Sharma, A. Ambadi, N. Hegde, J. Whiteaker, R. McLaughlin, H. Gardner, P. Madhavapeddi, V. Ramachandran, P. Kaur, A. Narayan, S. Guptha, D. Awasthy, C. Narayan, J. Mahadevaswamy, K. Vishwas, V. Ahuja, A. Srivastava, K. Prabhakar, S. Bharath, R. Kale, M. Ramaiah, N. Choudhury, V. Sambandamurthy, S. Solapure, P. Iyer, S. Narayanan, M. Chatterji, Azaindoles: noncovalent DprE1 inhibitors from scaffold morphing efforts, kill *Mycobacterium tuberculosis* and are efficacious in vivo, *J. Med. Chem.* 56 (2013) 9701.
- [10] P. Shirude, P. Madhavapeddi, M. Naik, K. Murugan, V. Shinde, R. Nandishaiah, J. Bhat, A. Kumar, S. Hameed, G. Holdgate, G. Davies, H. McMiken, N. Hegde, A. Ambady, J. Venkatraman, M. Panda, B. Bandodkar, V. Sambandamurthy, J. Read, A Methyl-thiazoles: a novel mode of inhibition with the potential to develop novel inhibitors targeting InhA in *Mycobacterium tuberculosis*, *J. Med. Chem.* 56 (2013) 8533.

- [11] P. Shirude, R. Shandil, M. Manjunatha, C. Sadler, M. Panda, V. Panduga, J. Reddy, R. Saralaya, R. Nanduri, A. Ambady, S. Ravishankar, V. Sambandamurthy, V. Humnabadkar, L. Jena, R. Suresh, A. Srivastava, K. Prabhakar, J. Whiteaker, R. McLaughlin, S. Sharma, C. Cooper, K. Mdluli, S. Butler, P. Iyer, S. Narayanan, M. Chatterji, Lead optimization of 1,4-azaindoles as antimycobacterial agents, *J. Med. Chem.* 57 (2014) 5728.
- [12] M. Panda, S. Ramachandran, V. Ramachandran, P. Shirude, V. Humnabadkar, K. Nagalapur, S. Sharma, P. Kaur, S. Guptha, A. Narayan, J. Mahadevaswamy, A. Ambady, N. Hegde, S. Rudrapatna, V. Hosagrahara, V. Sambandamurthy, A. Raichurkar, Discovery of pyrazolopyridones as a novel class of noncovalent DprE1 inhibitor with potent anti-mycobacterial activity, *J. Med. Chem.* 57 (2014) 4761.
- [13] S. Stanley, S. Grant, T. Kawate, N. Iwase, M. Shimizu, C. Wivagg, M. Silvis, E. Kazyskaya, J. Aquadro, H. Hung, Identification of novel inhibitors of *M. tuberculosis* growth using whole cell based high-throughput screening, *ACS Chem. Biol.* 7 (2012) 1377.
- [14] T. Christophe, M. Jackson, H. Jeon, D. Feinstein, J. Kim, A. Genovesio, J. Carralot, F. Ewann, S. Lee, E. Park, W. Shin, R. Brosch, S. Cole, P. Brodin, High content screening identifies decaprenyl-phosphoribose 2' epimerase as a target for intracellular antimycobacterial inhibitors, *PLoS Pathog.* 5 (2009) e1000645.
- [15] F. Wang, D. Sambandan, R. Halder, J. Wang, S. Batt, B. Weinrick, I. Ahmad, P. Yang, Y. Zhang, J. Kim, M. Hassani, S. Huszar, C. Trefzer, T. Kaneko, K. Mdlili, S. Franzblau, A. Chatterjee, K. Johnsson, K. Milkusova, G. Besra, K. Futterer, S. Robbins, W. Bames, P. Schultz, Identification of a small molecule with activity against drug-resistant and persistent tuberculosis, *PNAS* 27 (2013) E2510.
- [16] S. Batt, T. Jabeen, V. Bhowruth, L. Quill, P. Lund, L. Eggeling, L. Alderwick, K. Futterer, G. Besra, Structural basis of inhibition of *Mycobacterium tuberculosis* DprE1 by benzothiazinone inhibitors, *PNAS* 109 (2012) 11354.
- [17] R. Chikhale, R. Bhole, P. Khedekar, K. Bhusari, Synthesis and pharmacological investigation of 3-(substituted 1-phenylethanone)-4-(substituted phenyl)-1, 2, 3, 4-tetrahydropyrimidine-5-carboxylates, *Eur. J. Med. Chem.* 44 (2009) 3645.
- [18] R. Chikhale, A. Pant, S. Menghani, P. Wadibhasme, P. Khedekar, Facile and efficient synthesis of benzoxazole derivatives using novel catalytic activity of PEG-SO₃H, *Arabian J. Chem.* (2014), <http://dx.doi.org/10.1016/j.arabjc.2014.06.011>.
- [19] R. Chikhale, A. Pant, S. Menghani, P. Wadibhasme, P. Khedekar, Development of dual inhibitors targeting DprE1 and AHAS for treatment of *Mycobacterium tuberculosis* infection, *BMC Infect. Dis.* 14 (2014) 2–4, <http://dx.doi.org/10.1186/1471-2334-14-S3-E24>.
- [20] M. Naik, V. Humnabadkar, S. Tantry, M. Panda, A. Narayan, A. Guptha, V. Panduga, P. Manjrekar, L. Jena, K. Koushik, G. Shanbhag, S. Jatheendranath, M. Manjunatha, G. Gorai, C. Bathula, S. Rudrapatna, V. Achar, S. Sharma, A. Ambady, N. Hegde, J. Mahadevaswamy, P. Kaur, P. Sambandamurthy, D. Awasthy, C. Narayan, S. Ravishankar, P. Madhavapeddi, J. Reddy, K. Pabhakar, R. Saralaya, M. Chatterji, J. Whiteaker, B. McLaughlin, L. Chiarelli, G. Riccardi, M. Pasca, C. Binda, J. Neres, J. Dhar, F. Signorino-Gelo, J. McKinney, V. Ramachandran, R. Shandil, R. Tommasi, P. Iyer, S. Narayanan, V. Hosagrahara, S. Kavanagh, N. Dinesh, S. Ghorpade, 4-aminoquinolone piperidine amides: noncovalent inhibitors of DprE1 with long residence time and potent antimycobacterial activity, *J. Med. Chem.* 57 (2014) 5419.
- [21] F. Mir, S. Shafi, M.S. Zaman, N. Kalita, V.S. Rajput, C. Mulakayala, N. Mulakayala, I.A. Khan, M.S. Alam, Sulfur rich 2-mercaptobenzothiazole and 1,2,3-triazole conjugates as novel antitubercular agents, *Eur. J. Med. Chem.* 76 (2014) 274.
- [22] R. Jayaram, S. Gaonkar, P. Kaur, B. Suresh, B. Mahesh, R. Jayshree, V. Nandi, S. Bharat, R. Shandil, E. Kantharaj, V. Balasubramanian, Pharmacokinetics-pharmacodynamics of Rifampin in an aerosol infection model of tuberculosis, *Antimicrob. Agents Chemother.* 47 (2003) 2118.
- [23] A. Marry, G. De, C. Janet, L. Colby, J. Elizabeth, K. Lisa, G. Veronica, A. Charles, M. Lan, J. Anne, Comparative studies evaluating mouse models used for efficacy testing of experimental drugs against *Mycobacterium tuberculosis*, *Antimicrob. Agents Chemother.* 55 (2011) 1237.
- [24] K. Takacs-Novak, A. Avdeel, Interlaboratory study of log P determination by shake-flask and potentiometric methods, *J. Pharm. Biomed. Anal.* 4 (1996) 1405.
- [25] C. Gao, T. Ye, N. Wang, X. Zeng, L. Zhang, Y. Xiong, X. You, Y. Xia, Y. Xu, C. Peng, W. Zuo, Y. Wei, L. Yu, Synthesis and structure-activity relationships evaluation of benzothiazinone derivatives as potential anti-tubercular agents, *Bioorg. Med. Chem. Lett.* 23 (2013) 4919.
- [26] G. Riccardi, M. Pasca, L. Chiarelli, G. Manina, A. Mattevi, C. Binda, The DprE1 enzyme, one of the most vulnerable targets of *Mycobacterium tuberculosis*, *Appl. Microbiol. Biotechnol.* 97 (2013) 8841.
- [27] A. Liav, E. Swiezewska, E. Ciepchal, P. Brennan, Stereoselectivity in the synthesis of polypropenylphosphoryl β-d-ribofuranoses, *Tetrahedron Lett.* 47 (2006) 8781.
- [28] SAINTPLUS, Bruker AXS Inc., Madison, Wisconsin, USA, 2003.
- [29] G. Sheldrick, SADABS, Program for Empirical Absorption Correction, University of Gottingen, Gottingen, Germany, 1996.
- [30] G. Sheldrick, SHELX-97, Programs for Crystal Structure Analysis, University of Gottingen, Gottingen, Germany, 1997.
- [31] V. Barve, F. Ahmed, S. Adsule, S. Banerjee, S. Kulkarni, P. Katiyar, C. Anson, S. Powell, S. Padhye, F. Sarkar, Synthesis, molecular characterization, and biological activity of novel synthetic derivatives of chromen-4-one in human cancer cells, *J. Med. Chem.* 49 (2006) 3800.
- [32] F. Martins, S. Santos, C. Ventura, R. Elvas-Leitao, L. Santos, S. Vitorino, M. Reis, V. Miranda, H. Correia, J. Aires-de-Sousa, V. Kovalishyn, D. Latino, J. Ramos, M. Viveiros, Design, synthesis and biological evaluation of novel isoniazid derivatives with potent antitubercular activity, *Eur. Med. Chem.* 81 (2014) 119.
- [33] V. Makarov, G. Manina, K. Mikusova, U. Mollmann, O. Ryabova, B. Saint-Joanis, N. Dhar, M. Pasca, S. Buroni, A. Lucarelli, A. Milano, E. De Rossi, M. Belanova, A. Bobovska, P. Dianiskova, J. Kordulakova, C. Sala, E. Fullam, P. Schneider, J. McKinney, P. Brodin, T. Christophe, S. Waddell, P. Butcher, J. Albrethsen, I. Rosenkrands, R. Brosch, V. Nandi, S. Bharath, S. Gaonkar, R. Shandil, V. Balasubramanian, T. Balganes, S. Tyagi, J. Grosset, C. Riccardi, S. Cole, Benzothiazinones kill *Mycobacterium tuberculosis* by blocking Arabinan synthesis, *Science* 324 (2009) 5928.
- [34] S. Magnet, R. Hartkoorn, R. Szekeley, J. Pato, J. Triccas, P. Schneider, C. Szantai-Kis, L. Orfi, M. Chambon, D. Banfi, M. Bueno, G. Turcatti, G. Keri, S. Cole, *Tuberculosis* 90 (2010) 354.
- [35] C. Thierry, J. Mary, K. Hee, Denis, C. Monica, K. Jaeseung, G. Auguste, C. Jean-Philippe, E. Fanny, H. Eun, Y. Sae, K. Sunhee, J. Min, J. Eun, S. Henrieta, P. Ha, R. Giovanna, N. JiYoun, M. Laurent, K. Marie, J. Marie-Laure, O. Taegwon, K. Won, N. Zaesung, N. Ulf, B. Roland, T. Stewart, B. Priscille, New prospects for research on manipulation of insect vectors by pathogens, *PLoS Pathog.* 5 (2009) 1.
- [36] S. Ajmani, K. Jadhav, A. Kulkarni, Three-dimensional QSAR using the k-nearest neighbor method and its interpretation, *J. Chem. Inf. Model* 46 (2006) 24.